XAFS study of the low-temperature tetragonal phase of $La_{2-x}Ba_xCuO_4$: Disorder, stripes, and T_c suppression at $x=0.125$

D. Haskel* and E. A. Stern
Department of Physics, University of Washington, Seattle, Washington 98195-1560

F. Dogan
Department of Materials Science and Engineering, University of Washington, Seattle, Washington 98195-2120

A. R. Moodenbaugh
Division of Materials Science, Brookhaven National Laboratory, Upton, New York 11973
(Received 23 July 1999; revised manuscript received 14 October 1999)

Angular dependent x-ray absorption fine structure (XAFS) measurements of all La, Ba, and Cu sites determined the origin and nature of the intrinsic disorder present in the low temperature tetragonal (LTT) structural ground state of $La_{2-x}Ba_xCuO_4$ with $x=0.125,0.15$ at $T=10$ K. Ba doping induces major local distortions that extend as far as 5 Å from its lattice site. Despite the low Ba content the large distortions significantly affect the XAFS of the *majority* La and Cu sites. The distribution of the local LTT tilt angle of CuO_6 octahedra was directly determined from single and multiple scattering contributions to the XAFS of La and Cu sites. This angle, which regulates the strength of electron-lattice and spin-spin coupling in this material, was found to exhibit large, random fluctuations with rms $[\langle(\theta-\langle\theta\rangle)^2\rangle]^{1/2}\approx 2\langle\theta\rangle$, $\langle\theta\rangle$ being the average tilt angle determined by diffraction techniques. These fluctuations originate in the large, random, static disorder introduced with Ba doping. Their presence has implications for the plausibility of a mobility gap causing T_c suppression at $x=0.125$ in only the LTT phase, and for the correlation length of the postulated charge and spin stripes.

I. INTRODUCTION

The low-temperature tetragonal (LTT) structural ground state that occurs for most of the x values at which high-T_c superconductivity is observed in $La_{2-x}Ba_xCuO_4$ has been the subject of many investigations since it was first described by Axe *et al.*[1] The interest in obtaining detailed information on this structural modification has recently grown, partly due to the strong electron (hole)-lattice coupling that is experimentally observed in this (but no other) structural modification of La-based cuprates. This strong coupling is manifested for $La_{1.875}Ba_{0.125}CuO_4$ as a clear upturn of the resistivity[2,3] and anomalies in the Hall coefficient, thermoelectric power, and magnetic susceptibility[3] that coincide with the structural phase transition into the LTT phase at $T\approx 60$ K. In addition to these normal state anomalies, high-T_c superconductivity is strongly reduced at $x=0.125$. The enhanced hole-lattice coupling could also be crucial for the formation of periodic, static, charge stripes, which are observed by neutron-scattering studies in isostructural $La_{1.48}Nd_{0.4}Sr_{0.12}CuO_4$, also a suppressed superconductor.[4,5] In this compound, partial Nd substitution for La stabilizes the LTT phase, pinning the stripes as their period becomes commensurate with the lattice modulation at $x\sim 1/8$.[4]

Pressure and doping experiments[6,7] have been instrumental in revealing the direct influence of the LTT phase on the electronic properties. Applying pressure to, or doping Sr into $La_{1.875}Ba_{0.125}CuO_4$, stabilize the low-temperature orthorhombic (LTO) structure with a concomitant enhancement of the otherwise suppressed superconductivity. Oxygen reduction (which removes two holes per oxygen atom) in $La_{2-x}Ba_xCuO_{4-y}$ and Thorium doping (which removes one hole per Th atom) in $La_{2-x-z}Th_zBa_xCuO_4$ show that the sharp suppression of superconductivity depends on doping and is centered about the critical-hole concentration of $h_c=x-2y=x-z\approx 0.125$.[8,9] Whereas it is clear from an experimental standpoint that both $h_c\sim 0.125$ and an underlying LTT phase result in enhanced hole-lattice coupling and effectively reduce T_c, quite physically distinct mechanisms are suggested to explain the observed T_c suppression.

One such model is based on local-density-functional (LDA) calculations by Pickett, Cohen and Krakauer[10] (PCK), which show that in the LTT phase a gap occurs along a Brillouin zone edge (the M–A edge) precisely at the Fermi energy (E_F) for $x\sim 0.125$, destroying much of the Fermi surface. This band splitting originates in the different electron (hole) energies associated with the two inequivalent, in-plane and out-of-plane, $O_{x,y}$ sites that result from the CuO_6 octahedra tilts of the LTT phase ($O_{x,y}$ are oxygens forming the basal plane of CuO_6 octahedra). The redistribution (in energy) of electronic states due to band splitting reduces the density of states (DOS) at E_F for $x=0.125$ by about a factor of two[10] and splits a van Hove singularity (VHS). Since doping with Ba tunes E_F to the minimum in the split VHS (in a rigid band picture) at $x=0.125$, a qualitative explanation for the observed T_c suppression is obtained.

A related mechanism is proposed by Barišić and Zelenko (B&S),[11] in which charge transfer between the inequivalent planar oxygen sites leads to a charge density wave (CDW) ground state that stabilizes the LTT phase. In this scenario the resultant CDW competes with superconductivity for the Fermi surface. Whereas in B&S the instability is electronic

in origin (Peierls-like), it is likely that an ionic instability also contributes to stabilize the LTT phase,[10] as the CuO_6 octahedra tilts of the LTT phase result in major changes in La-O_z configuration (O_z form the apices of CuO_6 octahedra and reside in La_2O_2 planes) *and* inequivalent $O_{x,y}$ sites that promote charge transfer and CDW formation.

The plausibility of the PCK model has been questioned by Norman *et al.*,[12] as the magnitude of the LTT tilt angle of CuO_6 octahedra required to split the VHS is significantly larger (by about a factor of two) than the experimental value determined by diffraction techniques.[13–16] By using this experimental value in their linearized muffin-tin orbital calculations, Norman *et al.* show that the VHS remains nearly intact in the LTT phase while it does split as per PCK when the larger tilt angles are introduced. Since the interaction between octahedral tilts and electrons is quadratic in tilt angle,[11,17] the occurrence of band splitting and related dip in the DOS is very sensitive to its value. It is therefore important, in order to assess the applicability of the PCK model, to obtain detailed experimental information on the magnitude of CuO_6 octahedra tilts. As we show in Secs. III B 1 and III B 2, we were able to obtain the first and second moments of the tilt-angle distribution from analysis of partial pair and three-body correlations in atomic positions, which determine single- and multiple-scattering XAFS signals.

The segregation of doped holes into periodically spaced charge stripes, which are antiphase boundaries for antiferromagnetically ordered domains has been observed by neutron-scattering experiments[4] in the LTT phase of the suppressed superconductor $La_{1.48}Nd_{0.4}Sr_{0.12}CuO_4$. Pinning of charge stripes by the LTT lattice modulation at $x\sim 1/8$ is suggested as the reason behind T_c suppression,[18,19] while dynamically fluctuating stripes[4,18,19] are suggested to coexist with bulk superconductivity in La-based cuprates away from $x\sim 1/8$. As indicated by Emery and Kivelson,[20,21] the ordered arrangement of charge stripes is different from the Peierls-like Fermi-surface instability that drives a CDW ground state. Stripe formation arises from frustrated phase separation due to a competition between long-range Coulombic interaction, which tries to keep the holes uniformly distributed, and short-range interactions, which try to condense the doped holes into charge stripes allowing the preservation of the exchange energy in the antiferromagnetic arrangement of the undoped system.[20,21]

In $La_{1.875}Ba_{0.125}CuO_4$ the existence of charge and spin stripes and, to what extent they spatially order has not been established. The unavailability of large single crystals of $La_{2-x}Ba_xCuO_4$ has prevented the collection of reliable neutron-scattering data in this system. However, the observation in zero-field muon-spin-rotation (ZF-μSR) studies[22,23] of local magnetic order of Cu spins in $La_{1.875}Ba_{0.125}CuO_4$ similar to that measured in striped $La_{1.48}Nd_{0.4}Sr_{0.12}CuO_4$ provides strong circumstantial evidence in favor of spin stripe ordering in $La_{1.875}Ba_{0.125}CuO_4$. The size of the ordered local Cu moment derived from the μSR studies[23] is about three times larger than the value obtained in the neutron-scattering studies,[24] likely indicating the presence of disorder in the direction and/or phase of the spin modulation.[23,18] Disorder more strongly affects the long-range neutron probe than the μSR local probe. Additional evidence for local stripe order comes from recent ^{63}Cu nuclear quadrupole resonance (NQR) measurements.[25] A wipeout of the NQR intensity is observed below the LTO to LTT structural phase boundary for both $La_{1.875}Ba_{0.125}CuO_4$ and $La_{1.48}Nd_{0.4}Sr_{0.12}CuO_4$, the wipeout fraction closely following the order parameter for charge stripe ordering found in the neutron scattering studies of the latter compound. With new evidence suggesting that disorder plays an important role in determining the topology of spin and charge stripe ordering in La-cuprates, it is important to obtain detailed structural information on the local scale to gain insight into the origin of such disorder.

For charge stripes pinned by the lattice at $x\sim 0.125$, local, static, atomic displacements commensurate with the charge ordering occur. Assuming that these displacements involve only breathing motions of $O_{x,y}$ oxygens in a direction perpendicular to the stripes, Tranquada *et al.*[24] estimated the amplitude of the ordered in-plane modulation to be ≈ 0.004 Å (rms displacement 0.0028 Å) in $La_{1.48}Nd_{0.4}Sr_{0.12}CuO_4$. Recent measurements on the same material[18] provide evidence that disorder is present in the charge stripe spacing. Therefore the above estimate, which is based on the contribution of the ordered component of the lattice modulation to the charge order-superlattice peak intensity, is a lower limit for the amplitude of local displacements.

The ability of XAFS to detect local displacements that accompany charge ordering is, of course, dependent upon their magnitude. For in-plane displacements the distribution of planar Cu-$O_{x,y}$ distances will broaden to reflect the varying bond lengths that occur along the modulated charge density. The XAFS signal at the Cu site is a weighted average over all such sites and therefore includes sites in both the charge-stripes and the magnetic-stripes. As in all wave phenomena, the ability to resolve distances in XAFS (i.e. spatial resolution) is determined by the maximum photoelectron (p.e.) wavenumber, $k_{\max}$, available in the data (minimum p.e. wavelength). The smallest splitting in interatomic distances that can be *resolved* (distinguished as two separate distances) is given by $\delta r\sim \pi/2k_{\max}$; i.e., a difference in p.e. phase shift of $\approx\pi$ is needed (in XAFS the p.e. travels twice the interatomic distance between absorber and scatterer before recombining with its outgoing part at the absorber). $k_{\max}$ is limited by both atom vibrations and the reduction in the backscattering amplitude. For the La-cuprates at low temperatures, typically $k_{\max}\approx 15$ Å^{-1} limiting the spatial resolution to about $\delta r\approx 0.1$ Å.

If charge-stripes form in $La_{1.875}Ba_{0.125}CuO_4$ with atomic displacements similar in amplitude to those in the ordered charge modulation of $La_{1.48}Nd_{0.4}Sr_{0.12}CuO_4$ (therefore, below the XAFS spatial resolution), they will only manifest in XAFS as a slight increase in mean-squared relative displacement (MSRD), σ^2, of the distribution of Cu-$O_{x,y}$ bonds, of $\approx 8\times 10^{-6}$ Å^2. We note that XAFS measures the MSRD in bond length while the estimates in Ref. 24 are for mean-squared displacements in oxygen positions relative to the lattice sites, u^2. However, even assuming a similar magnitude for Cu displacements and complete anticorrelated motion of Cu and O atoms the increase in σ^2 would be only 3×10^{-5} Å^2.[26] Currently available theoretical standards used in XAFS analysis have limited accuracy for calculating XAFS amplitudes.[27] This introduces systematic errors in the

derived, amplitude-related, structural parameters in addition to errors introduced by the analysis procedure (such as background subtraction). For ordered structures this limits the accuracy in the measurement of σ^2 to about $(1-5)\times 10^{-4}$ Å^2. The increased disorder is therefore expected to be undetected by XAFS. Even the much larger modulation found in $La_2NiO_{4.125}$ (amplitude ~ 0.018 Å),[28] if ordered, will be difficult to detect by XAFS. However, if a large component of the atomic displacements is random (e.g., due to disorder in the stripe spacing) it may manifest itself in the σ^2 measured by XAFS (such random disorder may also be observed in diffuse scattering experiments). Recent XAFS measurements[29] at the Cu *K*-edge of powder samples of $La_{2-x-y}Sr_x(Eu,Nd)_yCuO_4$ found no detectable increase in Cu-$O_{x,y}$ disorder at the onset of the stripe ordering. This indicates that, even if a random component of displacements exists, the above small estimates still hold for (Nd, Eu) doped cuprates.

Here we report in Sec. III E on *angular-dependent* XAFS measurements on magnetically aligned powders of $La_{2-x}Ba_xCuO_4$ allowing us to separate the in-plane, Cu-$O_{x,y}$, from the out-of-plane, Cu-O_z, pair correlations enhancing the sensitivity for detection of in-plane distortions. The temperature dependence we obtain for the disorder in these pair correlations shows no detectable anomaly (within our uncertainties) below the temperature of formation of the LTT phase. From our results we are able to put an upper limit of ≈ 0.017 Å on the rms disorder in Cu-$O_{x,y}$ distances introduced by postulated stripes in $La_{2-x}Ba_xCuO_4$, for both $x=0.125,0.15$ samples. Since XAFS measures the instantaneous atomic distribution around the absorbing atom (averaged over all such atoms)[30] it cannot distinguish between static and dynamically fluctuating stripes. We discuss in Sec. IV the implications of local structural disorder present in the LTT phase, particularly the large, static, spatial variations in the tilt angle of CuO_6 octahedra.

II. EXPERIMENTAL DETAILS

A. Sample preparation: synthesis and magnetic alignment of powders

Powders of $La_{2-x}Ba_xCuO_4$ ($x=0.125,0.15$) were synthesized by the combustion technique to achieve a high grade of chemical homogeneity. Starting compounds, the appropriate mixtures of La, Ba, and Cu nitrates, were dissolved in water along with the appropriate amount of sucrose to obtain a highly concentrated solution. The solution was first dried followed by a combustion reaction on a hot plate. The precursor powders were then calcined at 900 °C in air and pressed into cylindrical pellets about 3 g each. The melting temperature of the powders was 1180 °C, as determined by thermogravimetrical analysis. Sintering of samples took place in air at 1140 °C for 4 days in order to achieve a larger grain size that facilitates the procedure of magnetic alignment of powders, as discussed below. The sintered samples were slowly cooled at a rate of 1 °C/min to room temperature. Grain size in the sintered pellets, observed in a scanning electron microscope, was ≈ 5 μm.

For the oriented XAFS measurements we used magnetically aligned powder. Obtaining a high degree of alignment requires powder composed predominantly of single crystallites so that their easy axis of magnetization, the $\hat{c}$ axis in the normal, paramagnetic state of $La_{2-x}Ba_xCuO_4$,[31] becomes aligned with the applied magnetic field. Based on the ≈ 5 μm grain size of sintered pellets and, assuming that grain boundaries are weak links so that polycrystalline samples preferentially break along them, grinding, together with size discrimination should result in the vast majority of powder particles being single crystals.

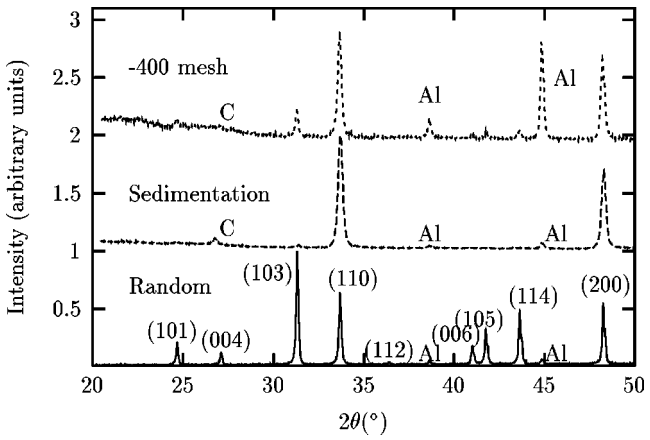

FIG. 1. X-ray powder diffraction from random and aligned $La_{1.875}Ba_{0.125}CuO_4$ at RT. Aluminum (Al) peaks (sample holder) and (002) reflection of graphite powder (C) also shown. Bragg reflections are labeled within the *I*4/*mmm* tetragonal space group; note enhancement of $(h,k,0)$ reflections in aligned sample. Only partial alignment is obtained for -400 mesh powders due to significant fraction of nonsingle crystalline grains.

Fine powder was obtained by sedimentation of ground specimens in dehydrated alcohol. The top layer composed only of small particles was then extracted (particle size $1-3$ μm observed under an optical microscope). The fine powder was mixed with about 20% (by volume) graphite powder ($\lesssim 2$ μm size) prior to thoroughly mixing with the Buehler© thermoplastic cement used as the embedding medium for alignment. Mixing in graphite helps prevent particle agglomeration, which results from the large surface to volume ratio of the fine powder and related surface charging. The mixture was cast into a disk in an aluminum frame, sealed with kapton tape and placed in a superconducting magnet with $B=8$ T parallel to the disk face. Heating to about 120 °C in the field causes the cement to soften allowing the particles to rotate so that their $\hat{c}$ axis is parallel to the magnetic field; within the $\widehat{ab}$ plane the orientation is random. Subsequent cooling to room temperature in the field hardens the cement and constrains the particles in the preferred orientation.

Figure 1 shows x-ray powder diffraction data of random and aligned powder. The scattering geometry is such that the x-ray momentum transfer is perpendicular to the plane of the disk (containing the $\hat{c}$ axis in the aligned sample) and therefore only $(h,k,0)$ reflections would contribute if alignment was perfect. The relative enhancement/suppression of the (110)/(103) peaks relative to random powder indicates the sample is very well aligned. We estimate the fraction of alignment from *ratios* of measured intensities in random and aligned powders to be $\gtrsim 95\%$. As we show later, a consistent, independent, estimate of the degree of alignment is ob-

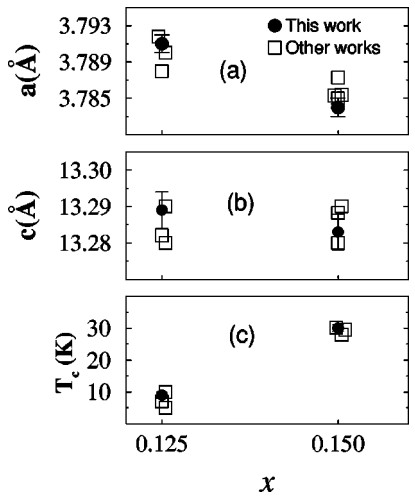

FIG. 2. (a)–(b) Room-temperature lattice parameters determined from refinements of x-ray powder diffraction; (c) Bulk onset T_c's determined from magnetization measurements. Representative values from the literature also shown (Refs. 2, 14, and 34).

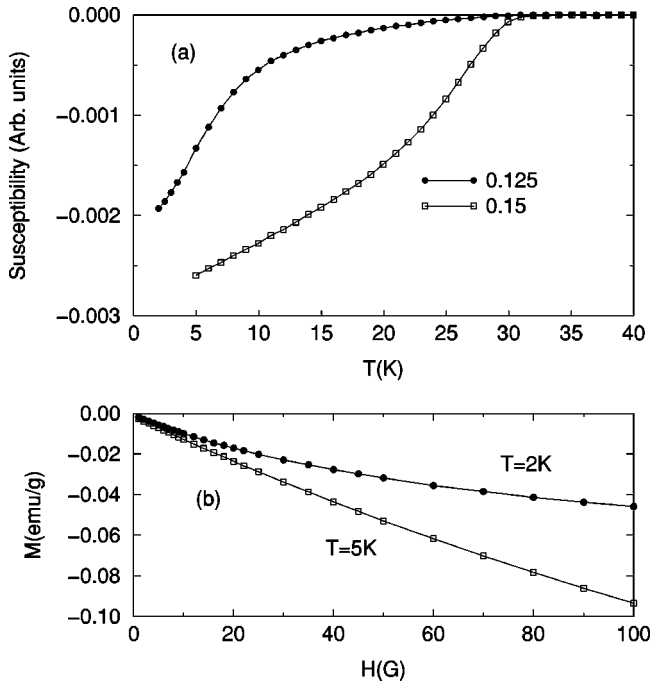

FIG. 3. Magnetization measurements of fine powders of $La_{2-x}Ba_xCuO_4$: (a) ZFC magnetic susceptibility. (b) Magnetization vs applied field curves used in estimating apparent superconducting volume fraction. Powder particle size is comparable to penetration depth (~ 1 μm) resulting in broad diamagnetic transitions and small apparent superconducting volumes.

tained from fits to the Cu *K*-edge XAFS data. We note that the enhancement of $(h,k,0)$ reflections in our samples is much smaller than what it would be for a single crystal, as the alignment procedure results in $(h,k,0)$ planes that are randomly oriented *around* the $\hat{c}$ axis. In addition, a measure of the mosaic spread of aligned grains was obtained from rocking curves of both (110) and (200) peaks, which show a full width at half maximum (using Cu K_α radiation) of 3.4(2)° and 2.6(2)°, respectively. These values are similar to those reported by Hyun, Sanders, and Finnemore[32] for magnetically aligned powders of $Nd_{1.85}Ce_{0.15}CuO_4$.

We emphasize the importance of having powder composed mostly of single crystallites in Fig. 1 where we show results obtained when ground specimens were sieved through -400 mesh (opening 38 μm) instead of using the sedimentation method, resulting only in partial alignment.

B. Sample characterization: Lattice parameters and T_c measurements

Structural and superconducting information was obtained on the fine powders used for the XAFS measurements. Lattice parameters were refined at room temperature by nonlinear least-squares fitting of 15 reflections of the $I4/mmm$ tetragonal space group. The refined values are shown in Fig. 2 and are in good agreement with values reported in the literature.[2,14,33]

Superconducting transition temperatures were obtained from dc magnetic susceptibility measurements using a Quantum Design MPMS© superconducting quantum interference device magnetometer. Samples were cooled in zero field (ZFC) followed by heating in a nominal $H=1$ Gauss applied field. Immediately after ZFC measurements, samples were measured on cooling in the same field (FC). FC data are within 5% (smaller diamagnetic response) of those of ZFC so we only show the latter in Fig. 3. The lack of complex topology in the fine powder sample composed mostly of single crystalline grains explains the similarity of FC and ZFC results; i.e., flux pinning is a small factor. Bulk onset T_c values, defined as the temperature at which the normal state (practically zero) susceptibility intercepts the extrapolated steepest slope of the transition, are also shown in Fig. 2 and compared with values of other workers.[2,14,34]

Both samples show a diamagnetic response starting at $T \sim 30$ K; the broad onset for $x=0.125$ has been observed by other workers[2,14] and is attributed to a small fraction (few %) of the sample becoming superconducting at this temperature. We also show in Fig. 3 M/H curves for both samples. The apparent superconducting volume fractions are given by the slopes of these curves at low magnetic fields. The ideal diamagnetic response for a 100% superconducting volume is given by $\chi_{\text{ideal}}=M/H=-1/4\pi\rho=-1.1\times10^{-2}$ emu/g, with $\rho=7.06$ g/cm^3. The slope of M/H curves (at low fields) indicates an apparent superconducting volume fraction of $\approx 7\%$ and 10% for $(x=0.125,0.15)$, respectively (no corrections for demagnetization factors are applied). These low fractions are due to the powder crystallite size being comparable to the penetration depth, $\lambda(T)$. Similarly low apparent superconducting volume fractions were obtained by Nagano *et al.*[35] using powders of ~ 2 μm of the closely related $La_{2-x}Sr_xCuO_4$ system; there $\lambda(0)\approx 1$ μm.[35,36] From Fig. 3 we find the lower critical field $H_{c1}(T)$, above which vortex lines penetrate the sample reducing the superconducting volume fraction, to be $H_{c1}(2\text{ K})\lesssim 20$ G (for $x=0.125$) and $H_{c1}(5\text{ K})\lesssim 30$ G (for $x=0.15$). For additional discussion of apparent superconducting volume in related compounds, see Refs. 37 and 38.

The value of $T_c\approx 10$ K for the $x=0.125$ sample is close to the higher end of T_c values obtained for this composition.[2,14,34] Often samples at this composition are de-

scribed as ''suppressed superconductors'' or ''nonsuperconducting.'' In fact all samples measured by us show a clear superconducting transition with onset above 2 K. The actual onset temperature varies from a low of ≈ 2.5 K up to the ≈ 10 K for the present sample. We have no direct evidence for why T_c varies between samples. Since the LTT structure appears to be influenced by microstructural features,[39] we suspect that grain size, twin and/or grain boundary configuration may play a role. It is also possible that the T_c is somewhat higher due to a slight deficiency in oxygen content, of $\delta \leqslant 0.005$ in $La_{2-x}Ba_xCuO_{4-\delta}$.[2,14] While we cannot rule out this possibility, the samples were cooled in air at a rate of 1 °C/min., slow enough to typically produce nominally fully oxidized samples. The minor effect that such oxygen reduction would have on the structural properties at $x=0.125$ is discussed by Takayama *et al.*[14] and includes a shift of about 10 K- to higher temperature- of the LTT-LTO phase boundary. The possibility of our nominal $x=0.125$ sample being fully oxygenated but having a slightly different Ba content was considered (e.g., $T_c \sim 10$ K for $x \sim 0.11$), but found less likely due to the increased disagreement between the measured lattice parameters and those corresponding to a different Ba content.[2,14]

To summarize, lattice parameters and T_c values are in good agreement with those of other workers and give an upper limit to oxygen deficiency in our $x=0.125$ sample of $\delta=0.005$ *or* an uncertainty in Ba content $\delta x=0.01$.

C. XAFS measurements

XAFS measurements were performed in transmission at beam line X-11A of the National Synchrotron Light Source (NSLS) using Si(111) (Cu *K*-edge) and Si(311) (La, Ba *K*-edges) double crystal monochromators. Harmonics at the Cu *K*-edge were rejected by detuning the second crystal so as to reduce the intensity of the fundamental by $\approx 20\%$; no detuning was applied for the (Ba, La) *K*-edges as the intensity of the NSLS synchrotron radiation at the energy of their third harmonic, ≈ 120 KeV, is negligible. Samples were put in a gas tight copper cell with Kapton windows and indium seals, filled with He gas for thermal exchange and attached to a displex refrigerator cold finger.

Energy resolution was optimized at the different energies by limiting the vertical divergence of the beam before and after the double crystal monochromator. Premonochromator slits, about 20 m away from source, were set to 1 mm and 0.5 mm for Cu and (Ba,La) *K*-edges, respectively. For the Cu *K*-edge with Si(111) crystals we estimate $\Delta E \approx 2.5$ eV; for the La *K*-edge with Si(311) $\Delta E \approx 16$ eV. For comparison, the core-hole lifetime broadenings of the Cu and La *K*-edges are ~ 2 and ~ 20 eV, respectively.[40]

Angular dependent XAFS spectra were measured by rotating the samples relative to the electric field vector of the synchrotron radiation, which is nearly 100% linearly polarized in the plane of the orbit. Special care was taken during the measurements to ensure that the sample position remains in the plane of the orbit and that the acceptance angle determined by the slits' apertures is such that no significant contribution is obtained from the out-of-plane component of polarization. The angular distribution of intensity with in-plane and out-of-plane electric field components depends on energy.[41] Premonochromator slits of ~ 1 mm at a distance of ~ 20 m from the source define an elevation angle of $\psi \sim 0.025$ mrad. At the Cu *K*-edge, the intensity of the in-plane polarized component, integrated up to $\psi=0.025$ mrad is $\approx 97\%$ of the total intensity. At the higher energies of Ba and La *K*-edges this percentage is even higher[41] and the radiation allowed by the angular aperture of the slits can be considered fully polarized in the plane of the orbit. During the measurement the height of the beam before the premonochromator slits is monitored by a position sensitive ion-chamber detector.

Different amounts of sample material corresponding to thicknesses of $t=350$, 98, and 16 μm for Ba, La, and Cu *K*-edges, respectively, were used for the different absorption edges to account for their different absorption lengths in $La_{2-x}Ba_xCuO_4$ (Ba *K*-edge 250 μm, La *K*-edge 72 μm and Cu *K*-edge 6 μm). The particle size of the fine powder used in our samples ($\sim 1-3\,\mu m$) is much smaller than the sample thickness for all edges minimizing thickness distortions.[42] The variation in sample thickness over an area of several mm is less than 10%, as verified from changes in the absorption edge step.

III. DATA ANALYSIS AND RESULTS

A. General remarks

The cross section for photoelectric x-ray absorption past an absorption edge of a deep core atomic state in condensed matter exhibits energy dependent fine structure due to modification of the photoelectron (p.e.) final state (at the position of the absorbing atom) introduced by scattering from neighboring atoms. For *K*-edges $(1s)$ in single scattering (SS) and harmonic approximations, this fine structure (XAFS) is given by[43,44]

$$\chi(k) = -\sum_j 3(\hat{\epsilon}\cdot\hat{r}_j)^2 \frac{S_0^2 N_j F_j(\pi,k,r_j)}{kr_j^2} \times e^{-2k^2\sigma_j^2} e^{-2r_j/\lambda(k)} \sin[2kr_j + \delta_j(k,r_j)], \quad (1)$$

where k is the p.e. wavenumber measured relative to the Fermi level, $S_0^2 N_j$ an effective coordination number that includes changes in passive electrons wave functions due to the presence of the core hole, F_j a curved wave backscattering amplitude, σ_j the root mean-squared relative displacement in interatomic distance, λ an effective mean-free path, which includes the finite lifetime of the core hole, r_j the interatomic distance, δ_j an overall scattering phase shift, and $\hat{\epsilon}$ the x-rays polarization vector. The sum is over all possible single-scattering paths. The generalization of Eq. (1) to multiple scattering (MS) includes considering *effective* scattering amplitudes and phases (which depend on the geometry of the scattering path) and an appropriate account of the polarization dependence.[45–47] A Fourier transform of $\chi(k)$ in Eq. (1) with respect to $2k$ can be related to the *partial* radial and angular atomic distribution function about the absorbing atom. The ability of SS and MS XAFS to obtain *partial* pair and three-body correlations is particularly important for the case here, in which La and Ba occupy the same crystallographic site and yet their local environments were separately determined by tuning the x-ray energy to the characteristic

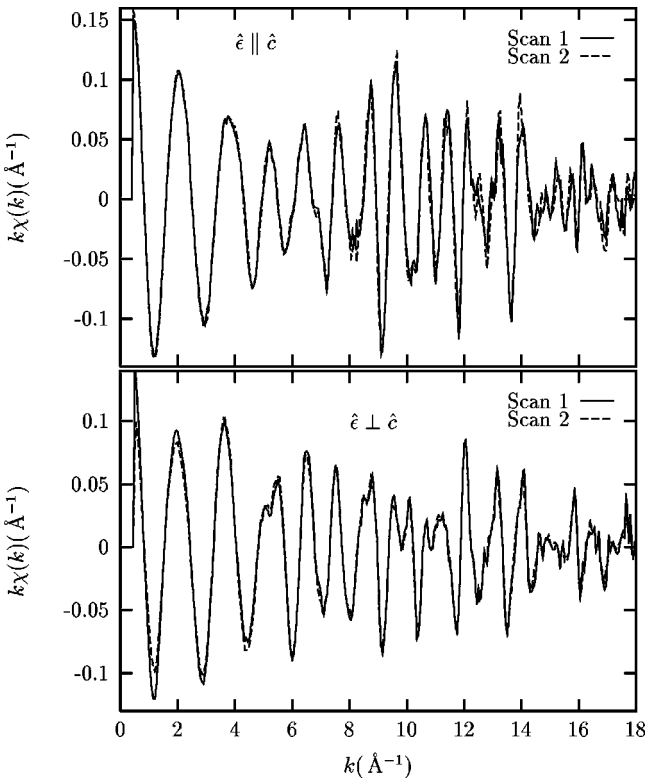

FIG. 4. The XAFS, $k\chi(k)$, of the La K-edge in $La_{1.875}Ba_{0.125}CuO_4$ at $T=10$ K. Two scans are shown for each polarization. Statistical errors are small (as seen from the high reproducibility); errors in the derived structural parameters are mostly of systematic nature, as discussed below.

threshold of each atom. In contrast, diffraction techniques yield an average of the La/Ba environments, dominated by the La majority atoms. The anisotropic layered structure of $La_{2-x}Ba_xCuO_4$ results in large angular dependence of $\chi(k)$ relative to the x-rays' polarization, which is exploited here to help resolve the local structure around all probed atoms.

Figure 4 shows representative $\chi(k)$ data (weighted by k) obtained at the La K-edge of $La_{1.875}Ba_{0.125}CuO_4$, for $T=10$ K (LTT phase) and electric field vector parallel and perpendicular to the $\hat{c}$ axis.

The data, $\chi^{\text{exp}}(k)$, were analyzed using the UWXAFS analysis package.[48] XAFS data for electric field parallel and perpendicular to the $\hat{c}$ axis are analyzed *concomitantly*. This allowed reducing the number of fitting parameters relative to the number of independent points in the data, as fitted structural parameters of scattering paths that contribute in both polarization conditions are constrained to be the same. FEFF6 theoretical code, which includes multiple-scattering contributions,[47] was used to calculate $F_j(k), \delta_j(k), \lambda(k)$, and polarization dependence based on the known average structure.[13,14] A theoretical $\chi^{\text{th}}(k)$ is constructed whose adjustable structural parameters r_j, σ^2, α (α buckling angle of nearly collinear MS paths) are refined against the experimental data by nonlinear least-squares minimization of a reduced χ^2_ν statistic,[48]

$$\chi^2_\nu = \frac{N_I}{\nu N} \sum_{i=1}^{N} \left(\frac{|\tilde{\chi}^{\text{th}}(r_i) - \tilde{\chi}^{\text{exp}}(r_i)|}{\epsilon(r_i)} \right)^2, \tag{2}$$

where the sum is over all pairs of points (real and imaginary parts of the difference are evaluated) in the fitted region of Fourier transformed r-space. Here $N_I = (2\Delta k \Delta r)/\pi + 2$ is the number of independent points in the fitted region,[49] $\nu = N_I - N_P$ the degrees of freedom in the fit, and $\epsilon(r_i)$ the evaluated uncertainty in the numerator's difference of Eq. (2). An estimate for ϵ is obtained from the rms value of $\chi^{exp}(r)$ in the range 15–25 Å, where the XAFS is assumed to be indistinguishable from the random noise. This underestimates the uncertainty since it does not include systematic errors in the data *and* theory. Whereas a good fit should result in $\chi^2_\nu \approx 1 \pm \sqrt{2/\nu}$,[48,50] the missevaluation of ϵ obscures the interpretation of χ^2_ν for the goodness of fit, typically resulting in $\chi^2_\nu \gg 1$. To aid with this, a fractional misfit R is evaluated,[50]

$$R = \frac{\sum_{i=1}^{N} |\tilde{\chi}^{\text{th}}(r_i) - \tilde{\chi}^{\text{exp}}(r_i)|^2}{\sum_{i=1}^{N} |\tilde{\chi}^{\text{exp}}(r_i)|^2}. \tag{3}$$

A small value of R together with $\chi^2_\nu \gg 1$ indicates that systematic errors dominate the uncertainty and rescaling $\epsilon \rightarrow \epsilon(\chi^2_\nu)^{1/2}$ recovers the $\chi^2_\nu \approx 1$ criteria for a good fit. Uncertainties in the parameters, which are calculated by the change needed to increase χ^2_ν by $1/\nu$ from its minimum value (1 standard deviation) and include the effect of correlations between fitting parameters, are rescaled by $(\chi^2_\nu)^{1/2}$. Two fits with similar values of ν are significantly different (2 standard deviations) if the ratio $\chi^1_\nu/\chi^2_\nu \gtrsim (1+2\sqrt{2/\nu})$, the fit with the lowest χ^2_ν being better. The fits presented here have $R \lesssim 0.03$ and $10 \lesssim \chi^2_\nu \lesssim 40$. Assuming errors are randomly distributed and therefore can be added in quadrature, $\epsilon^2 \approx \epsilon^2_{\text{ran}} + \epsilon^2_{\text{sys}} \approx \epsilon^2_{\text{ran}}\chi^2_\nu \Rightarrow \epsilon_{\text{sys}} \approx \epsilon_{\text{ran}}(\chi^2_\nu - 1)^{1/2} \approx \epsilon_{\text{ran}}\chi_\nu$ indicating that systematic errors are ~ 3–6 times bigger than statistical errors.

Coordination numbers, N_j, are set in the fits to the values of the average structure. Additional fitting parameters are S_0^2 and an overall E_0 shift to adjust the $k=0$ reference between experiment and theory.

B. La *K*-edge results

1. Direction of local CuO_6 octahedra tilts in LTT phase and first moment of tilt angle distribution

The sensitivity of XAFS to changes in local tilt *direction* is mainly at the La site, as the distribution of La-O(2), planar, interatomic distances is strongly dependent on tilt direction (Fig. 5). The resultant splittings, whose average values determined by diffraction[13,14,33] are included in Table I, are large enough to be resolved from our data. Since tilts are about Cu sites and almost rigid, Cu XAFS is nearly insensitive to the orientation of tilts.

It is evident from Table I that the complicated near-neighboring environment of the La site in the LTT phase (6 La-O distances) cannot be resolved by XAFS on a *randomly* oriented powder. The number of independent points in the first ''shell'' region of a powder XAFS spectrum for such structure is $N_I \approx (2\times 11 \times 0.8)/\pi \approx 6$ (assuming a usable

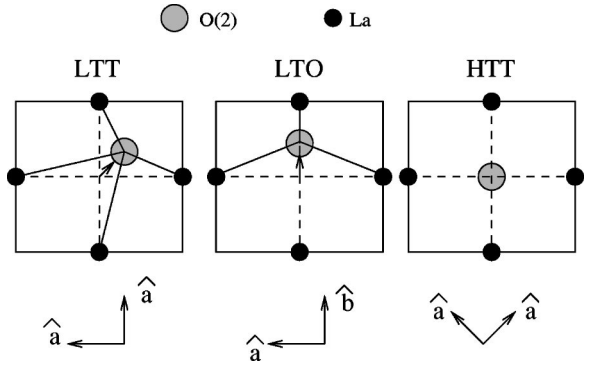

FIG. 5. Planar La-O(2) distances for CuO_6 octahedra tilts about $\langle 110\rangle$ (LTT, $P4_2/ncm$), $\langle 100\rangle$ (LTO, $Bmab$) and for the high-symmetry (HTT, $I4/mmm$) phases, left to right. O(2) are apex to octahedra centered about Cu in the CuO_2 neighboring plane. Small correlated La displacements not shown.

k-range of 3–14 Å $^{-1}$ for the low-Z oxygens). This is not enough to resolve the La-O environment as additional σ^2, S_0^2, and E_0 variables are needed. *Angular-dependent* XAFS in this anisotropic structure allows for selectively probing different subsets of atoms, which for the two orientations measured here doubles the amount of information.

For example, the planar La-O(2) distances contribute in a significant manner *only* for $\epsilon \perp \hat{c}$, the short La-O(2) apical distance *only* for $\epsilon \| \hat{c}$ and the La-O(1, 1′) distances in both polarizations. Since the spectra are refined together, the structural parameters of the latter are constrained to be the same for both polarization conditions [the polarization dependence of their amplitudes $(\hat{\epsilon}\cdot\hat{r}_j)^2$ in Eq. (1) is accounted for in the FEFF6 calculation].

Fits were performed in the 1.7–5.3 Å region of *r*-space including both SS and MS contributions. The rotation of CuO_6 octahedra in the LTT phase displaces O(1) atoms above and below the CuO_2 plane by the same amount resulting in equally shortened and elongated La-O(1) distances relative to the La-O(1′) ones (within 0.004 Å due to small off-center displacement of La atoms). We therefore varied a central distance [$r' =$ La-O(1′)] and a splitting $\Delta O(1)$ and constrained the La-O(1) distances to $r = r' \pm \Delta O(1)$, respectively. The two planar La-O(2) distances were varied independently. A single σ^2 was varied for all the La-O distances,

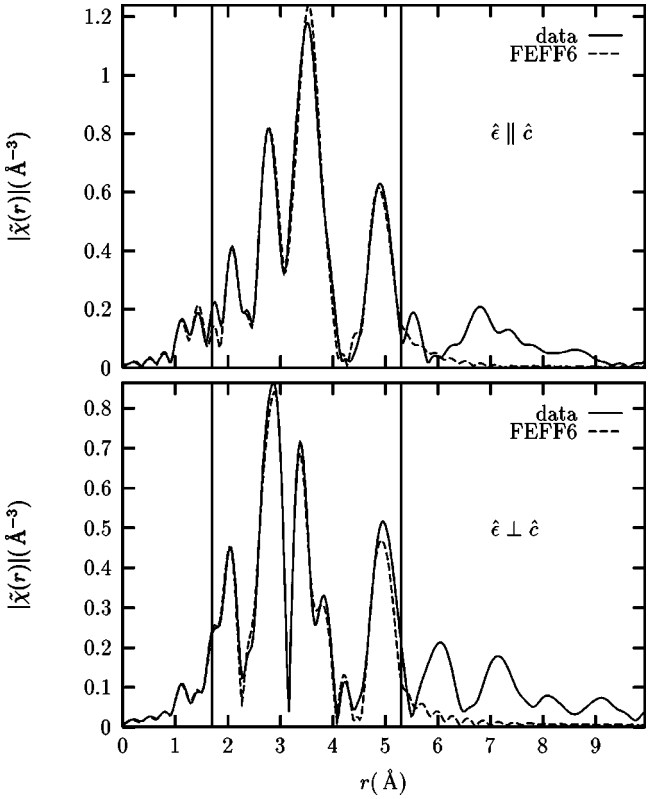

FIG. 6. Magnitude of the complex Fourier transform of $k^2\chi(k)$ using $k = 3-15$ Å $^{-1}$ XAFS data at the La *K*-edge for $x = 0.125$ at $T = 10$ K. Data and fit shown for both polarizations; vertical lines indicate fitting range. The degrees of freedom in the fits are $\nu = (N_I - N_P) = 59 - 25 = 34$. Goodness of fit parameters are $\chi_\nu^2 = 10.4$ and $R = 0.012$.

as a different σ^2 for the La-O(1,1′) distances was highly correlated with $\Delta O(1)$. This correlation is expected since the small splitting of $\Delta O(1) \approx 0.05$ Å found by diffraction can be approximated by an effective average distance together with an increase in σ^2 of $\approx 2.5\times10^{-3}$ Å ^{2}. Ba *K*-edge measurements verified that Ba substitutes at the La site (Sec. III D) and therefore scattering paths involving La, Ba backscatterers were weighted by their *nominal* concentrations $(1 - x/2)$, $(x/2)$, respectively.

La *K*-edge fits (Fig. 6) verified that the local tilts are about $\langle 110\rangle$ axis ($P4_2/ncm$ notation) in agreement with the dif-

TABLE I. Planar La-O(2) and La-O(1) distances as determined by neutron-diffraction studies (Refs. 13, 14, and 33). The O(1) oxygens are those in the Cu-O planes; in the LTT phase crystallographically inequivalent O(1) (out-of-plane) and O(1′) (in-plane) sites are formed due to octahedral rotations about Cu-O(1′) bonds.

Pair	LTT (Å)	LTO (Å)	HTT (Å)
La-O(2)	2.369	2.370	2.365
	2.616 (2×)	2.598	
	2.853 (2×)	2.731 (2×)	2.739 (4×)
		2.880	
La-O(1)	2.587	2.607 (2×)	
La-O(1′)	2.639 (2×)		
La-O(1)	2.695	2.675(2×)	2.649 (4×)

TABLE II. Fit results for interatomic distances (in Å) between La and neighboring atoms in $x=0.125,0.15$ samples at $T=10$ K as obtained from La *K*-edge polarized XAFS. Neutron-diffraction results are from Ref. 14. Coordination numbers given in parenthesis; the polarization in which each particular distance significantly contributes to the XAFS signal is also indicated. Nearly collinear multiple scattering (MS) paths also contribute to the XAFS near the Cu_{MS} and La_{MS} distances.

		Diffraction $x=0.125$	XAFS $x=0.125$	$x=0.15$
O(2)	$(\times 1)$, $\hat{c}$	2.369	2.353(14)	2.357(15)
O(1)	$(\times 1)$, $\hat{c},\hat{a}$	2.587	2.573(12)	2.574(11)
O(1′)	$(\times 2)$, $\hat{c},\hat{a}$	2.639	2.624(08)	2.625(10)
O(1)	$(\times 1)$, $\hat{c},\hat{a}$	2.695	2.673(12)	2.676(12)
O(2)	$(\times 2)$, $\hat{a}$	2.616	2.615(10)	2.626(10)
O(2)	$(\times 2)$, $\hat{a}$	2.853	2.872(12)	2.873(13)
Cu	$(\times 2)$, $\hat{c},\hat{a}$	3.229	3.235(03)	3.234(03)
Cu	$(\times 2)$, $\hat{c},\hat{a}$	3.263	3.282(03)	3.281(03)
La	$(\times 1)$, $\hat{c}$	3.683	3.682(05)	3.701(06)
La	$(\times 1)$, $\hat{a}$	3.723	3.746(10)	3.746(12)
La	$(\times 2)$, $\hat{a}$	3.781	3.776(05)	3.762(08)
La	$(\times 1)$, $\hat{a}$	3.838	3.866(10)	3.833(13)
La	$(\times 4)$, $\hat{c},\hat{a}$	3.969	3.975(04)	3.966(05)
Cu_{MS}	$(\times 1)$, $\hat{c}$	4.775	4.767(15)	4.748(17)
La_{MS}	$(\times 4)$, $\hat{c},\hat{a}$	5.278	5.262(17)	5.266(18)
La_{MS}	$(\times 4)$, $\hat{a}$	5.346	5.363(18)	5.333(20)

fraction results[13,14] and the pair distribution function (PDF) analysis of neutron-scattering data.[51] The refined planar La-O(2) distances are 2.615(10) Å and 2.872(12) Å, i.e., a splitting of $\Delta O(2)=0.252(16)$ Å compared to the 0.237(11) Å of the diffraction studies[14]. For the La-O(1) distances, $r'=2.624(8)$ Å and $\Delta O(1)=0.050(12)$ Å, compared to 0.054(10) obtained by diffraction. The uncertainties in the diffraction results include variations found in the literature.[13,14]

Table II summarizes near-neighboring distances up to ≈ 5 Å as obtained from the La *K*-edge XAFS analysis. The high quality of fits together with the excellent agreement between local and average structures at the La *K*-edge gives confidence in the methods presented here, including sample preparation procedures and data analysis.

Attempts to model the local structure at $T=10$ K within the LTO space group were unsuccessful. This is expected based on the large differences in planar La-O(2) distances between the LTT and LTO phases (Table I). When the interatomic distances are set to the values consistent with the LTO configuration the quality of fit (as determined by both χ^2_ν and *R* factor) is $\approx 100\%$ worse than the one obtained by setting the distances to those in the LTT phase.

We determined an upper limit to the fractional, local, LTO content in the LTT phase by fitting the planar La-O(2) XAFS signal with a mixture of LTT and LTO phases. A fractional LTO composition of $3.5\pm 10\%$ is obtained, without any improvement in the fit relative to the pure LTT phase. A similar result (within uncertainties) is obtained when such a mixture is allowed at the higher *r* values where the La-La (planar) pair correlations ($r\approx 3.78$ Å) contribute to the XAFS signal. The distribution of La-La (planar) distances is coupled to that of La-O(2) distances and is therefore quite different in the LTT and LTO phases.[13] We note that our result for the fractional LTO content is independent of whether an LTT or LTO model is used for the La-O(1) and La-O(1′) distances, as their differences are small and can be approximated by an ''effective'' distribution of four La-O(1) distances centered at $r\approx 2.64$ Å with a $\sigma^2\approx 2\times 10^{-3}$ Å^2. The essential information that unequivocally distinguishes between both phases is the planar La-O(2) distances. We conclude that the vast majority ($\gtrsim 95\%$) of local tilts at $T=10$ K are LTT-like for both $x=0.125,0.15$ samples. A similar upper limit for the fraction of LTO phase at $T=10$ K was obtained from both high-resolution x-ray diffraction[52] and PDF analysis of neutron-scattering data.[51]

From the splitting in La-O distances we can obtain the first moment of the local tilt angle distribution. The local tilt angle, *averaged over all* La *atoms* is $\langle\theta\rangle=3.3(4)°$, in excellent agreement with the 3.1(3)° value determined by diffraction techniques.[13,14] Evidence of disorder in the La environment, however, is seen by comparing the σ^2 in interatomic distances involving oxygen atoms to those obtained in the closely related Sr-doped system[53] (see Table III). Most striking is the increased disorder in the La-Cu_{MS} distance ($\hat{c}$ axis, $r\approx 4.77$ Å), which reflects the significant decrease of amplitude in the Fourier transformed XAFS at $r\approx 4.4$ Å, as shown in Fig. 7. Note that the ''peaks'' in the $2k$-Fourier transform of $\chi(k)$ [Eq. (1)] are shifted to the left from the actual distances r_j due to scattering phase shifts in the p.e. final state; i.e., $\partial\delta_j/\partial k<0$. Such a significant decrease in amplitude in the Ba-doped sample compared to the Sr-doped one is not expected based on the average structure results of

TABLE III. σ^2 (in Å^2) for different shell distances obtained from La *K*-edge XAFS in Ba-doped ($x=0.125$, $T=10$ K) and Sr-doped (Ref. 53) ($x=0.15$, $T=20$ K) La_2CuO_4. $S_0^2=0.93(6),0.95(6)$ for Ba- and Sr-doped samples, respectively, in agreement with the expectation that S_0^2 only depends on the absorbing atom type.

	O	Cu	La	Cu_{MS}
Sr	0.0020(10)	0.0020(4)	0.0019(5)	0.0035(10)
Ba	0.0053(11)	0.0019(3)	0.0023(2)	0.0078(20)

diffraction, as the LTO and LTT ground states of these samples differ mostly in the *direction* of octahedral tilts but not in their *magnitude*, rendering the contribution to the XAFS signal of nearly collinear, La-O(2)-Cu_{MS} MS paths essentially unchanged, as shown in the FEFF6 calculation of Fig. 7. These MS paths, whose amplitudes are strongly sensitive to the degree of collinearity of the three atom arrangement (buckling angle), contribute to the XAFS signal at nearly the same distance as the La-Cu_{MS} SS path.

As we show in the following sections, we are able to determine these three-body correlations directly from the data and, together with information from Ba and Cu *K*-edge XAFS analysis, to conclude that the decrease in amplitude at the La-Cu_{MS} distance is due to a broad distribution of local tilt angles about the average value $\langle\theta\rangle$, disorder that originates in the large difference in ionic size between the Ba dopant and La host atoms.

2. Second moment of local tilt angle distribution from La-O(2)-Cu MS paths

The atomic arrangement that determines the La-O(2)-Cu MS XAFS signal and its relation to CuO_6 octahedra tilts is schematically shown in Fig. 8. The p.e. wave excited at the La site undergoes, among others, single scattering (SS), double scattering (DS), and triple scattering (TS) events from nearly collinear O(2) and Cu atoms before its scattered portion recombines with its outgoing part at the position of the excited La atom. DS and TS involves one and two scattering events, respectively, from the intervening, bridging, O(2) atom in addition to scattering from the Cu end atom. Due to the small tilt angles of CuO_6 octahedra, DS and TS paths contribute to the XAFS signal at nearly the same distance as the SS path (4.773, 4.777, 4.781 Å for SS, DS, and TS paths, respectively).[13] The total signal at this distance is determined by the sum over these scattering contributions, each entering the sum with its own amplitude and phase.

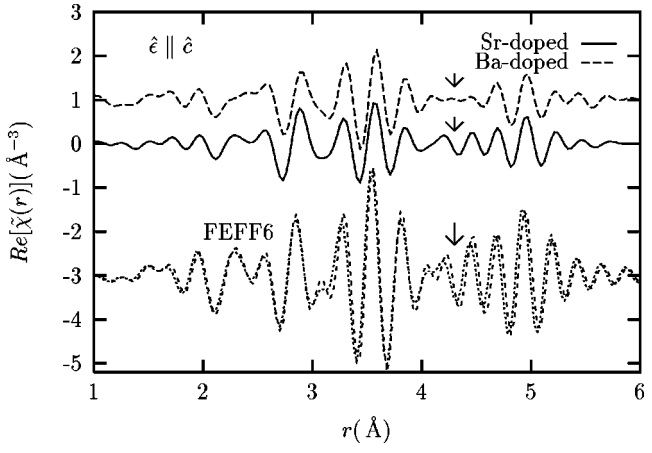

FIG. 7. Real part of the complex Fourier transform of $\hat{c}$-polarized La *K*-edge data in Sr ($x=0.15$, $T=20$ K) and Ba ($x=0.125$, $T=10$ K) doped cuprates. The large reduction in amplitude at the La-Cu_{MS} distance (arrows) in the Ba-doped sample is *not* due to the different structural ground states of these systems (LTO vs LTT) as shown by the FEFF6 $\hat{c}$-polarized calculation of both phases.

The sensitivity of La-O(2)-Cu MS XAFS to changes in buckling angle β is mostly due to the p.e. scattering amplitude at the intervening O(2) atoms being strongly peaked in the forward direction and rapidly decreasing with scattering angle. This results, for collinear paths, in an enhancement of the p.e. wave function at the position of the end atoms as compared to its value in the absence of the intervening, ''focusing'' atoms, enhancement that decreases as the deviation from collinearity increases.[45,54] The resultant three-particle correlation determines directly $\langle\beta^2\rangle$, which complements the indirect determination of $\langle\beta\rangle$ from the La-O distances, as explained below.

Scattering *amplitudes* of La-O(2)-Cu MS paths were parametrized in terms of buckling angle β by computing the effective scattering amplitude for several angles using FEFF6 theory and constructing a correction of the form $F_k(\beta)=F_k(\langle\beta\rangle)(\gamma_k+\zeta_k\beta^2)$. This functional form accurately describes the buckling dependence for $\beta\lesssim 20°$, as directly verified from fits of the β dependence of the theoretical $F_k(\beta)/F_k(\langle\beta\rangle)$ at several values of k (see Ref. 55). Here $\langle\beta\rangle$ is the average buckling angle found by diffraction tech-

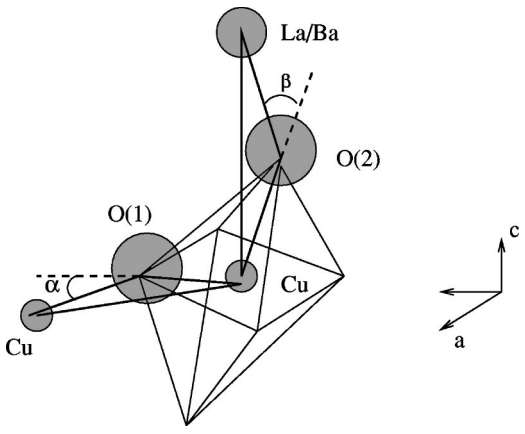

FIG. 8. Schematic representation of the MS paths used in determining tilt fluctuations about the $\hat{c}$ axis and $\widehat{aa}$ plane. La-O(2)-Cu correlations are determined from both La and Cu *K*-edge XAFS, Ba-Cu-O(2) correlations from Ba *K*-edge XAFS (Sec. III D) and Cu-O(1)-Cu correlations from Cu *K*-edge XAFS (Sec. III E).

TABLE IV. Einstein temperatures, static disorder $\sigma^2_{\rm off}$ and zero point ($T=10$ K) $\sigma^2_{\rm z.p.}$ (in Å^2) for La-Cu$_{\rm MS}$ as obtained from La K-edge XAFS in Sr-doped Ref. 53 ($x=0.15$) and Ba-doped ($x=0.125$) La_2CuO_4. $\langle\beta\rangle = 6.8°, 6.9°$ at $T=10$ K for Sr-doped (Ref. 57) and Ba-doped (Ref. 13) samples, respectively.

	β(deg.)	$\theta_E(K)$	$\sigma^2_{\rm off}$	$\sigma^2_{\rm z.p.}$
Sr	6.8	156(20)	0.0001(10)	0.0035(10)
Ba	6.9	255(70)	0.0060(20)	0.0084(20)
	$\beta(T)$	158(23)	0.0013(15)	0.0038(10)

niques and γ_k, ζ_k are k-dependent coefficients obtained by fitting the β dependence of $F_k(\beta)/F_k(\langle\beta\rangle)$ separately for DS and TS paths *and* for each value of k. DS and TS half-path lengths were parametrized in terms of β and the SS half-path length at nearly the same distance, both of which are varied in the fit in addition to a single σ^2. The effective scattering *phases* used are those corresponding to $\langle\beta\rangle$, which for the angles at hand results in systematic errors in distance determination of $\lesssim 0.005$ Å, as verified in our fits, but does not affect the measurement of the buckling angle.

Since XAFS measures the instantaneous distribution of atoms around the probe atoms, *averaged* over all such atoms, it gives $\langle F_k(\beta)\rangle = F_k(\langle\beta\rangle)(\gamma_k + \zeta_k\langle\beta^2\rangle)$, where the brackets indicate average over all La atoms. For an instantaneous local buckling angle that *randomly* deviates from its average value, $\beta = \langle\beta\rangle + \delta\beta$, diffraction techniques measure $\langle\beta\rangle$ ($\langle\delta\beta\rangle = 0$ when averaged over long range) whereas XAFS measures $\langle\beta^2\rangle = \langle\beta\rangle^2 + \langle\delta\beta^2\rangle$; i.e., XAFS can directly determine the second moment of the local tilt angle distribution $\langle\delta\beta^2\rangle = \langle(\beta - \langle\beta\rangle)^2\rangle = \langle\beta^2\rangle - \langle\beta\rangle^2$. If local fluctuations in buckling angle exist XAFS necessarily yields $\langle\beta^2\rangle^{1/2} > \langle\beta\rangle$. As we show in Sec. III D, this fluctuation is expected due to the large, random, local distortions introduced with Ba doping.

Since both σ^2 and buckling angle (β) fitting parameters affect the La-O(2)-Cu amplitude (although with different k-dependences), correlations between these parameters are expected. In addition to accounting for these correlations in determining uncertainties in the best fit values,[50] additional criteria are needed to assess the physical validity of a model. Here, such criteria include a physical temperature dependence of the vibrational disorder in interatomic distances, self-consistency between La, Cu, and Ba XAFS probes and making contact with the closely related Sr-doped system.

We fitted the La-O(2)-Cu XAFS signal at $T=10$, 80, 140, 200, and 270 K by constraining the *vibrational* part of σ^2 to follow an Einstein model[56] but allowing for a T-independent offset, $\sigma^2_{\rm off}$, to account for *static* disorder in the interatomic distances, i.e.,

$$\sigma^2 = \frac{\hbar^2}{2M_r K_B \theta_E}\coth\left(\frac{\theta_E}{2T}\right) + \sigma^2_{\rm off}, \tag{4}$$

with θ_E the Einstein temperature and M_r the reduced mass of La and Cu atoms (a single σ^2 is fitted for the SS and MS paths at nearly the same distance). In addition we used the β-parameterized form of $F_k(\beta)$ and of MS half-path lengths. Table IV compares fitting results obtained for Sr-doped[53] and Ba-doped samples, where for the latter we show the effect of fitting β instead of using its average structure value. Our best fits give $\langle\beta^2\rangle^{1/2} = 15.2 \pm 3°$ at $T=10$ K, compared to $\langle\beta\rangle = 6.9°$ found by diffraction. Since the local *first* moment $\langle\beta\rangle$ agrees with the diffraction value (Sec. III B 1), this results in a rms local fluctuation in buckling angle $\langle\delta\beta^2\rangle^{1/2} = 2.0(4)\langle\beta\rangle$. The same ratio holds for fluctuations in tilt angle, which is about twice smaller than the buckling angle (not exactly twice due to small differences in Cu-O(2) and La-O(2) bond lengths and small relative displacements of Cu, La end atoms).[13] This result is, within uncertainties, the same at all temperatures and for both $x=0.125$,0.15 samples.

By assuming that $\delta\beta = 0$ (i.e., $\beta = \langle\beta\rangle$) in the Sr-doped case ($x=0.15$), we obtained a negligible static disorder $\sigma^2_{\rm off}$ (Table IV) indicating that buckling angle fluctuations about its average value are small (if present, these fluctuations would reduce the XAFS amplitude, a reduction that can be partially compensated for by an increased $\sigma^2_{\rm off}$). This result also shows that the *vibrational* contribution to deviations in local buckling angle from its first moment value is small (the static offset giving an estimate for the size of this effect).

This result is expected since Sr-induced local distortions have a small spatial extent[58] becoming noticeable in the XAFS of the majority La sites only for $x > 0.15$.[53] Using $\beta = \langle\beta\rangle$ in the Ba-doped case, however, yields a large $\sigma^2_{\rm off} = 0.006(2)$ Å^2. As we shall see in Sec. III D, this value is too large to be accounted for by changes in half-path length of La-O(2)-Cu SS and MS paths due to Ba-induced distortions of La, Cu, and O(2) atoms (weighted by the Ba content), which is estimated at $\sigma^2_{\rm off} \approx 1\times10^{-3}$ Å^2. This large $\sigma^2_{\rm off}$ must therefore be compensating for (unaccounted) fluctuations in local buckling angle. When such fluctuations are allowed in the fits, we obtain a value of $\sigma^2_{\rm off}$ consistent with the measured Ba-induced distortions (Table IV); in addition we obtain a *vibrational* behavior of σ^2 (θ_E and zero-point motion) nearly identical to that of the Sr-doped case, indicating that the effective local force constants determining *thermal* disorder in La-O(2)-Cu configuration are about the same in both cases. We conclude that most of the static disorder in La-O(2)-Cu configuration is due to local deviations in buckling angle from its average value introduced with Ba-doping. A much smaller fraction of static disorder is of other origin, and includes changes in La-O(2)-Cu SS and MS half-path lengths due to Ba-induced distortions. A consistent result is obtained from the measurement of Cu-O(2)-La/Ba configuration in Cu K-edge XAFS, Sec. III E.

C. Temperature induced LTT → LTO → HTT structural phase transitions

It has been previously shown that the temperature-induced structural phase transition from LTO to HTT in $La_{2-x}Sr_xCuO_4$ is of order-disorder character; i.e., the local

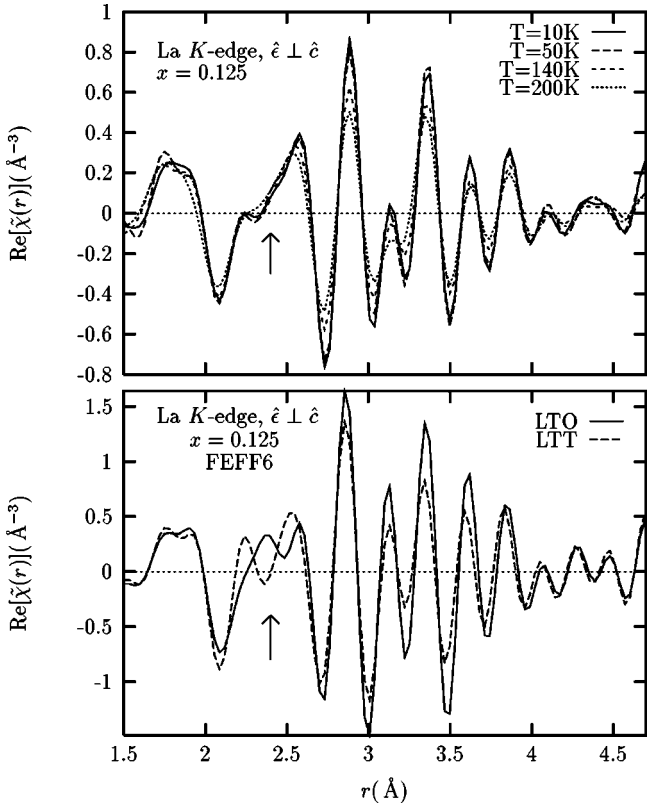

FIG. 9. Real part of the complex Fourier transform of $k^2\chi(k)$ using $k=3-14$ Å^{-1} XAFS data at the La K-edge for $x=0.125$, $\hat{\epsilon}\perp\hat{c}$ at several temperatures (top) together with FEFF6 calculation under same polarization conditions for the LTT and LTO structures (Ref. 13, bottom).

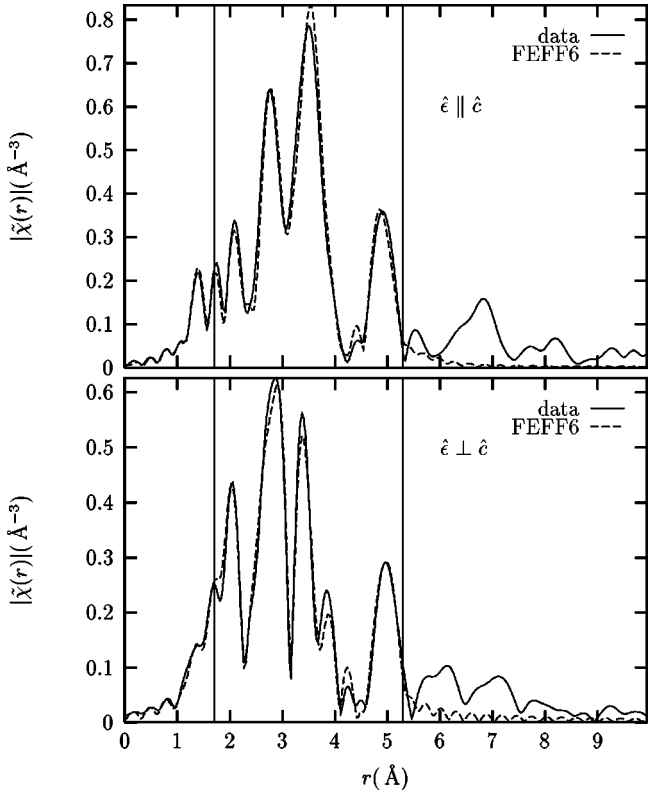

FIG. 10. Magnitude of the complex Fourier transform of $k^2\chi(k)$ using $k=3-14$ Å^{-1} XAFS data at the La K-edge for $x=0.125$ at $T=140$ K. Data and fit shown for both polarizations; vertical lines indicate fitting range. The degrees of freedom in the fits are $\nu=(N_I-N_P)=54-24=30$. Goodness of fit parameters are $\chi^2_\nu=9.5$ and $R=0.02$.

CuO_6 octahedra tilts do not vanish at the structural phase boundary but become disordered relative to each other to result in the zero tilt angle measured by diffraction techniques.[53,59] Similar order-disorder behavior was also reported for the LTT → LTO → HTT phase transitions in $La_{2-x}Ba_xCuO_4$ based on PDF analysis of neutron-scattering data.[51] It was found by Billinge, Kwei, and Takagi[51] that the CuO_6 octahedra do not change their *local* tilt direction from $\langle 110\rangle$ to $\langle 100\rangle$ at the LTT → LTO phase transition (Fig. 5) but rather tilt in the $\langle 110\rangle$ LTT direction at all temperatures. The LTO and HTT phases must therefore arise, it was argued, from superpositions of small (≈10 Å) domains with LTT symmetry.

Our XAFS results from La K-edge measurements on $La_{2-x}Ba_xCuO_4$ are in good agreement with these findings. The large rearrangement in planar La-O(2) distances that would have resulted from a change in local tilt direction at the LTT → LTO phase transition is not observed in our La K-edge, $\hat{a}$-polarized data, as shown in Fig. 9. Fitting results at $T=140$ K, significantly above the ≈60 K LTT → LTO transition, show that the local structure (≈5 Å scale) of both $x=0.125,0.15$ samples is well described by an LTT model with structural parameters nearly the same as those found at $T=10$ K (Fig. 10, Table V). An LTO model cannot describe the local structure within this length scale. A similar result is obtained within the HTT crystallographic phase (above about 200 K for $x=0.125$) for which a local HTT symmetry refinement yielded not only a bad fit but also an unphysically large σ^2 and planar La-O(2) distances, which are incompatible with the measured lattice parameters (Table V). In particular the local tilt angle does not vanish at the LTO → HTT phase transition. These results are in agreement with the PDF work, which found the LTT model best fits the data within a ≈4 Å scale at all temperatures, with a superposition of coherent local LTT variants giving a better fit at longer distances in the LTO and HTT phases.[51] The nearly temperature-independent fit values obtained in the refinements of buckling angles ($\langle\beta\rangle^2$, Secs. III B 2, III E) are consistent with the order-disorder nature of these phase transitions.

D. Ba *K*-edge results

1. Ba-induced local lattice distortions

In contrast to diffraction techniques, including the PDF analysis of neutron-scattering data, XAFS can distinguish the Ba environment from the La one as it measures the *partial* radial and angular atomic distribution function about the absorbing atom. If Ba substitutes at the La site without distorting its near-neighboring environment (as commonly assumed based on diffraction results), one expects their XAFS to be nearly the same (the absorbing atom's phase shifts are about the same due to their similar Z numbers). Figure 11 shows $k\chi(k)$ XAFS data obtained at the Ba and La K-edges for $x=0.125$ at $T=10$ K. The large differences are due to severe

TABLE V. La *K*-edge fit results for $x=0.125$ within the crystallographic LTO ($T=140$ K) and HTT ($T=270$ K) phases. La-O distances (in Å) and their σ^2 (in Å^2) are shown for different models, together with goodness of fit parameters χ^2_ν and *R*.

T(K)	140	270	270
Model	LTT	LTT	HTT
La-O(2)	2.353(10)	2.353(10)	2.360(20)
La-O(1)	2.550(11)	2.530(22)	
La-O(1′)	2.620(10) (×2)	2.610(20) (×2)	2.610(30) (×4)
La-O(1)	2.690(12)	2.700(23)	
La-O(2)	2.640(13) (×2)	2.630(18) (×2)	
La-O(2)	2.870(14) (×2)	2.860(20) (×2)	2.620(30) (×4)
σ^2	0.0055(14)	0.0059(16)	0.0156(20)
(χ^2_ν, *R*)	(9.5, 0.02)	(12, 0.03)	(21, 0.07)

local distortions around the Ba sites originating in its different charge state and much larger ionic size (1.47 Å ionic radius for Ba^{+2} versus 1.22 Å for La^{+3}, both 9-coordinated).[60] As revealed by our detailed analysis, these distortions can be represented as an expansion of the local atomic environment around Ba, with the size of the distortion decreasing with distance from the Ba site, as expected. The oxygen nearest neighbors are affected the most, which is reflected in Fig. 11 by the most significant changes seen in the lower frequency components (shorter distances) of the XAFS signal.

Refinements were carried out simultaneously for both polarizations, as described in Sec. III A. From fits of Ba *K*-edge data (Fig. 12), we confirmed that Ba substitutes at the La site but induces major distortions in its near-neighboring environment. These distortions are detectable (within a sensitivity of ≈ 0.01 Å) up to a radial distance of at least 5 Å from the Ba sites. Fit results are given in Tables VI and VII. Since the undistorted structure is highly anisotropic, with atomic ''shells'' consisting of more than one distance, atoms within such shells are affected differently. Though this results in an anisotropic expansion of the Ba surroundings (relative to the undistorted, average structure), we illustrate the effect of Ba substitution by showing angular-averaged ''shell'' distances and their radial displacements relative to

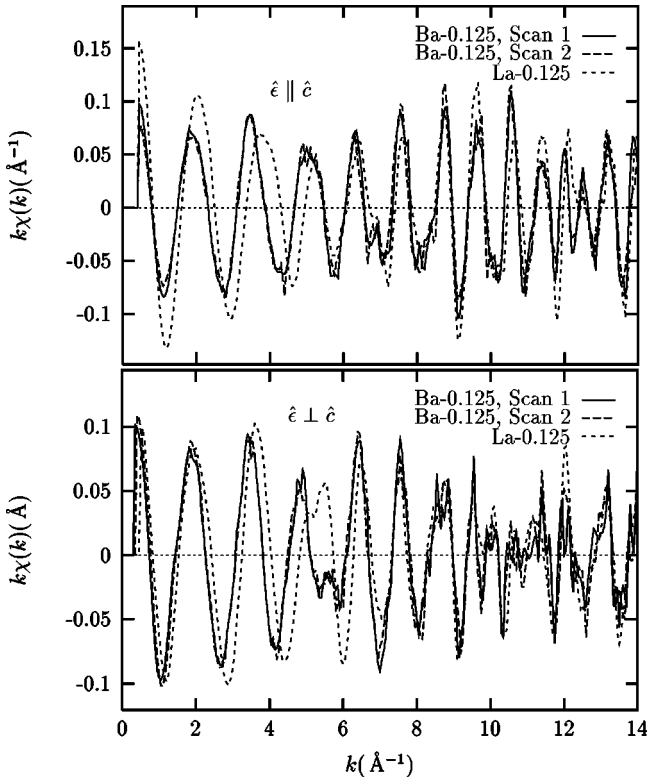

FIG. 11. XAFS signal $k\chi(k)$ at the Ba and La *K*-edges for $x=0.125$ at $T=10$ K. Reproducibility scans also shown for Ba data. The large differences, mostly at the lower frequencies (distances), indicate that Ba induces local distortions in its near-neighboring environment.

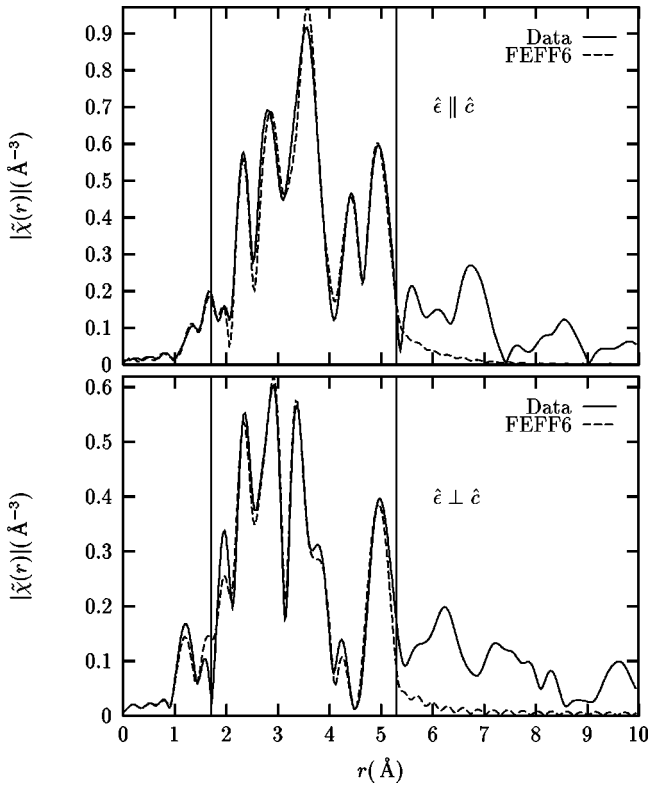

FIG. 12. Magnitude of the complex Fourier transform of $k^2\chi(k)$ using $k=3-14$ Å^{-1} XAFS data at the Ba *K*-edge for $x=0.125$ at $T=10$ K. Data and fit shown for both polarizations; vertical lines indicate fitting range. The degrees of freedom in the fits are $\nu=(N_I-N_P)=54-24=30$. Goodness of fit parameters are $\chi^2_\nu=13.1$ and $R=0.029$.

TABLE VI. Fit results for interatomic distances (in Å) between Ba and neighboring atoms in $x=0.125,0.15$ samples at $T=10$ K as obtained from Ba *K*-edge polarized XAFS. Coordination numbers given in parenthesis. Nearly collinear multiple scattering (MS) paths also contribute to the XAFS near the Cu_{MS} and La_{MS} distances.

	$x=0.125$	$x=0.15$
O(2) apical	2.540(13)	2.530(10)
O(1) (×2)	2.780(15)	2.760(15)
O(1) (×2)	2.797(15)	2.820(15)
O(2) planar	2.622(20)	2.648(20)
O(2) planar (×2)	2.871(10)	2.884(10)
O(2) planar	2.920(30)	2.895(26)
Cu (×2)	3.275(5)	3.267(5)
Cu (×2)	3.323(5)	3.314(5)
La apical	3.717(6)	3.722(7)
La planar	3.780(10)	3.782(10)
La planar (×2)	3.783(10)	3.783(8)
La planar	3.910(10)	3.903(8)
La (×4)	3.990(5)	3.981(5)
Cu_{MS}	4.790(10)	4.781(10)
La_{MS} (×4)	5.316(20)	5.311(17)
La_{MS} (×4)	5.371(20)	5.381(18)

the undistorted structure in Fig. 13.

The O(2) apical oxygen nearly along $\hat{c}$ is displaced away from Ba by 0.17(1) Å from its average position. Therefore, a weighted average of *local* Ba-O(2) [2.540(13) Å] and La-O(2) [2.353(14) Å] apical distances as obtained by XAFS gives $(1-x/2)\cdot 2.353+(x/2)\cdot 2.540=2.365(14)$ Å , in excellent agreement with the 2.369(2) Å *average* La/Ba-O(2) distance of diffraction.[14,13] Changes in Ba-O(1, 1′) distances relative to the average structure are in the [0.10 −0.18] Å range. Assuming O(1, 1′) displacements along the Ba-O(1, 1′) directions [the strong Cu-O(1, 1′) bonds would rather buckle than compress/expand] and, since these directions form ≈45° with the $\hat{c}$ axis, this introduces a $\hat{z}$ component of displacements of ≈0.1 Å . These displacements significantly alter the corrugation of the CuO_2 planes nearby a Ba dopant, as they introduce O(1′) displacements from the CuO_2 planes and change the buckling pattern of the already displaced O(1) atoms. For comparison, the $\hat{z}$ displacements of the latter in the undistorted structure are ≈ ±0.1 Å .[13,14]

The large oxygen displacements introduce local increases in the tilt angle of the CuO_6 octahedra that neighbor Ba dopants. The distortions, however, are not consistent with increased *rigid* tilts but rather with increased buckling with enhanced departures of the ∠(Cu-O(2), Cu-O(1, 1′) angles from 90°. Rigid tilts would have resulted in *contraction* of Ba-O(2) planar distances, while the opposite is observed. The significant distortions found for O(2)-planar, La-planar, La-apical, and Cu atoms would introduce disorder in the buckling configuration of La-O(2)-Cu_{MS} paths as well as introduce disorder in their scattering path lengths. Even assuming that the ≈0.05 Å Cu displacements are fully along $\hat{z}$, they will contract/expand (equally) La-O(2)-Cu_{MS} paths by about the same amount effectively introducing static disorder in their half-path lengths of about 2.5×10^{-3} Å^2. Each Ba atom affects 4 Cu atoms, which, at $x=1/8$ represents about 50% of their total, resulting in a weighted static disorder in La-O(2)-Cu_{MS} half-path lengths of about 1.25×10^{-3} Å^2. This is likely overestimated since the Cu displacements are not fully along $\hat{z}$. Other distortions contribute a much smaller amount of disorder in half-path length of these scattering paths. For example, the O(2)-planar and La-planar distortions would mostly contribute to disorder in the La-O(2)-Cu buckling angle configuration since displacements are mostly perpendicular to $\hat{z}$, i.e., to the p.e. direction of propagation. The Cu displacements will also contribute to disorder in this buckling angle, as they alter the relative positions of Cu and La end atoms.

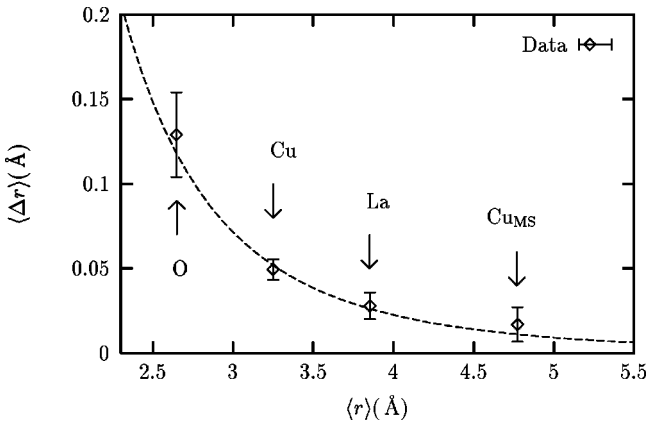

FIG. 13. The effect of Ba substitution on its near-neighboring environment. Angular-averages of both ''shell'' distances $\langle r\rangle$ and their radial atomic displacements $\langle\Delta r\rangle$ (relative to the undistorted average structure) are shown. Data corresponds to $x=0.125$ at $T=10$ K; dashed line is a guide to the eye.

As neighboring octahedra are coupled by their vortexes, one expects that these local distortions will extend into neighboring cells. Whereas XAFS cannot directly determine next-cell correlations due to the short p.e. mean-free path (≈5−10 Å), these will be short ranged as they are not detected in diffraction experiments. In addition, since Ba substitution is random, its distortions introduce random fluctuations in tilt angles about their average value. Since each Ba dopant occupies a sphere of radius $R\approx3.85c^{-1/3}$

TABLE VII. σ^2 (in Å^2) for different shell distances obtained from Ba *K*-edge XAFS of $x=0.125$, 0.15 samples at $T=10$ K; also $S_0^2=1.02\pm0.09$.

	O	Cu	La	Cu_{MS}
0.125	0.0045(12)	0.0034(3)	0.0035(2)	0.0025(5)
0.15	0.0044(13)	0.0036(3)	0.0037(2)	0.0029(9)

$=9.7$ Å (3.85 Å is a mean La-La distance and $c=0.0625$) and its distortions extend up to at least 5.5 Å (Fig. 13), a lower limit on the fractional volume that is affected by the Ba distortions is given by $(5.5/9.7)^3 \approx 18\%$. Next-cell correlations will enhance this fraction. As discussed above, however, a much larger fraction of *scattering paths* involving Cu and La atoms is affected by the Ba distortions. This large fraction is the reason behind our observation of significant disorder at the *majority* La and Cu sites.

2. Ba-O(2)-Cu three-body correlations

The same modeling procedure described in Sec. III B 2 was carried out here to determine the Ba-O(2)-Cu buckling angle distribution from the three body correlations that determine DS and TS paths. We fitted the Ba-O(2)-Cu XAFS signal at $T=10$, 140, and 270 K simultaneously, constraining the T-dependence of σ^2 to follow an Einstein model but allowing for static disorder in terms of an offset $\sigma^2_{\rm off}$, as described before. We compare models for which the buckling angle is set to its average structure value or otherwise independently refined. In clear contrast to the results for La-O(2)-Cu in Sec. III B 2, we obtained no significant static offset [$\sigma_{\rm off}=-0.0003(3)$ Å^2] by using the average value of $\beta=6.9°$ determined by diffraction. When allowed to vary, we obtained a smaller but consistent value of $\langle\beta^2\rangle^{1/2}_{\rm Ba}=5.4 \pm 1.7°$ at $T=10$ K with a $\sigma^2_{\rm off}=0.0008(6)$ Å^2. Both models yield an Einstein temperature $\theta_E=204(10)$ K (giving a zero-point motion $\sigma^2_{\rm z.p.}=0.0026(5)$ Å^2 at $T=10$ K).

The smaller *vibrational* disorder in the Ba-O(2)-Cu configuration compared to La-O(2)-Cu (Table IV) indicates a more rigid configuration for the former. This is not surprising since Ba substitution pushes (either due to electrostatic interaction, size effect, or both) the O(2)-apical *and* Cu_{MS} atoms away from it (Table VI), leaving less free space for the relative motions of Ba and Cu_{MS} atoms along the $\hat{c}$ axis. Since we cannot separately determine the local $\langle\beta\rangle_{\rm Ba}$ as we did for $\langle\beta\rangle_{\rm La}$, our results for $\langle\beta^2\rangle_{\rm Ba}=\langle\beta\rangle^2_{\rm Ba}+\langle\delta\beta^2\rangle_{\rm Ba}$ cannot distinguish between, e.g., a buckling distribution with $\langle\beta\rangle_{\rm Ba}=0$, $\langle\delta\beta\rangle_{\rm Ba}\neq 0$ or one with $\langle\beta\rangle_{\rm Ba}\neq 0$, $\langle\delta\beta\rangle_{\rm Ba}=0$. The former case, however, will put an *upper limit* on the size of fluctuations in buckling angle in the Ba-O(2)-Cu configuration of $\langle\delta\beta^2\rangle^{1/2}_{\rm Ba}=5.4\pm 1.7°=0.8(2)\langle\beta\rangle_{\rm La}$. Since for La-O(2)-Cu we obtained $\langle\delta\beta^2\rangle^{1/2}_{\rm La}=2.0(4)\langle\beta\rangle_{\rm La}$, we obtain that $\langle\delta\beta^2\rangle^{1/2}_{\rm Ba}=0.4(1)\langle\delta\beta^2\rangle^{1/2}_{\rm La}$; i.e., the rms buckling fluctuations in Ba-O(2)-Cu configuration is, at the most, half of its value for La-O(2)-Cu, expected since Ba atoms are well separated.

The significant differences between the more ordered Ba-O(2)-Cu three body correlations compared to the La-O(2)-Cu ones can be directly seen by their contribution to the amplitude of the Fourier transform of $\hat{c}$-polarized (La, Ba) *K*-edge data, as shown by the arrow in Fig. 14.

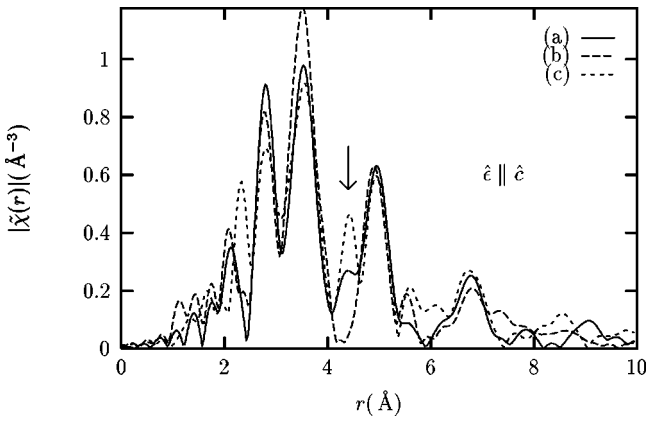

FIG. 14. Magnitude of the complex Fourier transform of $k^2\chi(k)$ using $k=3-14$ Å^{-1} data range for La *K*-edge in (a) $La_{1.85}Sr_{0.15}CuO_4$, $T=20$ K; (b) $La_{1.875}Ba_{0.125}CuO_4$, $T=10$ K and (c) Ba *K*-edge in $La_{1.875}Ba_{0.125}CuO_4$, $T=10$ K. The comparison is sound since Ba and La *K*-edge XAFS are broadened by nearly the same core-hole lifetime effects. The signal shown by the arrow reflects the fit results showing that Ba-O(2)-Cu signal has less disorder (thermal and static) than the La-O(2)-Cu signal in the Ba-doped samples and less thermal disorder compared to the La-O(2)-Cu signal of a Sr-doped sample.

E. Cu *K*-edge results

1. Temperature dependence of in-plane and out-of plane Cu-O correlations

The Cu site is the most suitable for investigating the local structure of the CuO_2 planes; in particular to establish whether anomalous behavior in their structural parameters is present that could correlate with the onset of spin/charge stripe ordering at low temperatures. As previously discussed, the ability of XAFS to resolve atomic displacements commensurate with stripe ordering is dependent upon their magnitude. Since by all estimates these displacements are near the detection limit of the XAFS technique, it is important to enhance the sensitivity to the signal of interest. Here, angular measurements on oriented powders allow us to separate in-plane Cu-O(1,1′) from out of plane Cu-O(2) correlations. Although this does not improve the theoretical ultimate spatial resolution (determined largely by $k_{\rm max}$, Sec. I), it eliminates background by isolating the planar and out-of-plane signals and increases the information content in the XAFS data; therefore enhancing our ability to resolve the local structure.

Cu *K*-edge data for $x=0.125$ at $T=10$ K is shown for both conditions of polarization in Fig. 15. Due to the simplicity of the nearest-neighboring environment of Cu sites compared to that of La/Ba sites we used Cu *K*-edge XAFS for a cross-check of the degree of alignment of our oriented powder. For this purpose, we fitted both polarizations simultaneously by assuming a fraction $1-p$ of perfectly oriented powder and a fraction p of misaligned powder. Irrespective of the two extreme cases assumed for the angular distribution of the latter relative to the polarization direction of the x-rays (random powder or ''antialigned'' powder, i.e., powder with its $\hat{c}$ axis *perpendicular* to the $\hat{c}$-axis orientation of fraction $1-p$) adding the fraction p in the r-space fits resulted in a worse fit and a fitted value $p=0.05(10)$, the uncertainty including variations between the different angular distributions assumed for fraction p. This is consistent with our estimates based on intensity ratios of Bragg reflections, Sec. II A, and verifies the fraction of misoriented powder in our samples to be $\lesssim 5\%$.

Fits were performed simultaneously for both orientations by constraining the structural parameters of those paths that

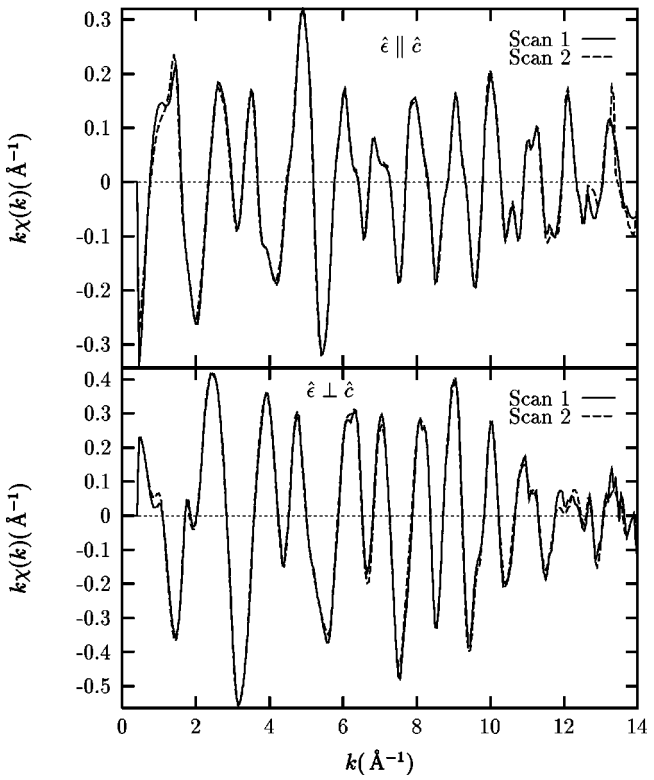

FIG. 15. Cu K-edge XAFS, $k\chi(k)$, of $La_{1.875}Ba_{0.125}CuO_4$ at $T=10$ K; two scans are shown for each polarization.

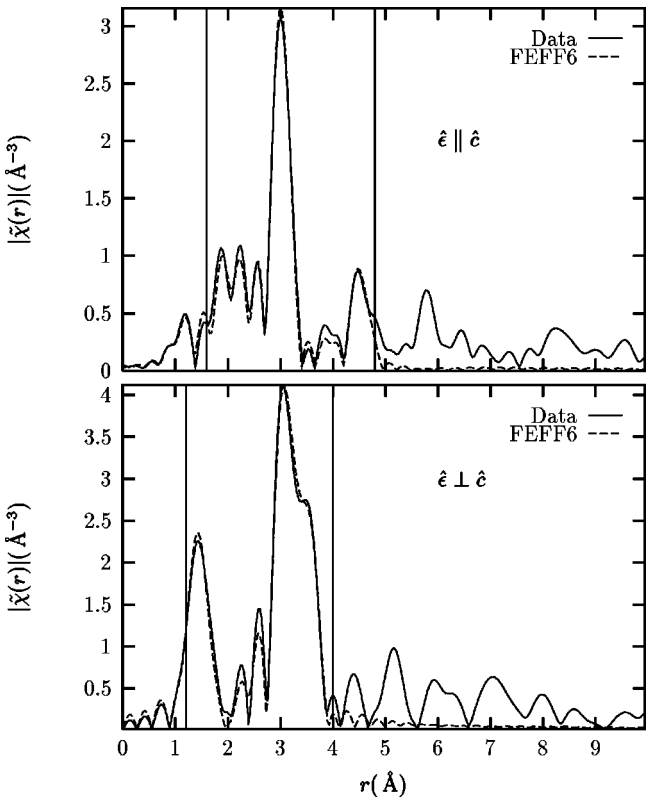

FIG. 16. Magnitude of the complex Fourier transform of $k^2\chi(k)$ using $k=3-14$ Å^{-1} XAFS data at the Cu K-edge for $x=0.125$ at $T=10$ K. Data and fit shown for both polarizations; vertical lines indicate fitting range. The degrees of freedom in the fits are $\nu=(N_I-N_P)=48-16=32$. Goodness of fit parameters are $\chi^2_\nu=40$ and $R=0.011$.

contribute in both polarizations (e.g., Cu-La SS paths). The average structure[13,14] has two distinct Cu-O(1′) and Cu-O(1) planar distances at 1.8902 Å and 1.8933 Å, respectively (LTT octahedral tilts are about the Cu-O(1′) direction displacing O(1) oxygens from the CuO_2 plane). Attempts to vary these distances independently resulted in large correlations with their σ^2 value and no improvement in the quality of fit as compared to using a single, double degenerate, distance. This is expected since such a small splitting cannot be resolved by XAFS (Sec. I) and can be effectively accounted for by a negligible, static contribution ($\approx 2.4\times10^{-6}$ Å^2) to the σ^2 of these bonds. A single Cu-O(1) planar distance was therefore varied, and any anomalous change (within the XAFS sensitivity) in the planar distribution of distances should manifest itself in deviations of this single distance or/and its σ^2 value from their expected temperature dependencies. A different σ^2 was refined for the Cu-O(1) and Cu-O(2) SS paths, as this significantly improved the fits. MS paths significantly contribute to the XAFS above $r\approx3.78$ Å ($\hat{a}$ polarization) and $r\approx4.77$ Å ($\hat{c}$ polarization) and their contributions were included. Data were refined at $T=10$, 30, 50, 80, 140, and 240 K. In order not to obscure any anomalous T-dependence of pair correlations, we initially fitted each temperature data set independently, without constraining their structural parameters to follow a predictated behavior (e.g., an Einstein model for the T-dependence of σ^2). Buckling angles of nearly collinear MS paths were initially constrained to the values dictated by the average structure.

Fit results are shown in Fig. 16. Temperature dependencies of selected interatomic distances and their σ^2 are shown in Figs. 17 and 18; the latter also includes fits of σ^2 values to Einstein models as per Eq. (4).

Self-consistency requires that the Cu-La distances and σ^2 obtained from the Cu K-edge analysis match the values obtained for the La-Cu distances in the analysis of La K-edge data (Table II), which is the case. For example, for $x=0.125$ at $T=10$ K the disorder in Cu-La/Ba bond lengths is $\sigma^2=0.0022(3)$ Å^2 compared to $\sigma^2=0.0019(3)$ Å^2 for the La-Cu bonds. The small differences are expected since Cu XAFS measures a weighted average of Cu-La/Ba correlations, while La XAFS determines La-Cu correlations only.

In Fig. 18, the large σ^2_{off} in the Cu-O(2) bond originates in the O(2) and Cu local distortions that occur near a Ba dopant, as described in Sec. III D 1. The La-O(2) and Ba-O(2) distances, as determined from La and Ba K-edge XAFS, differ significantly [2.353(14) Å, 2.540(13) Å]. Since La/Ba-O(2)-Cu_{MS} configurations are nearly collinear, from the measurements of La-Cu_{MS} [4.767(15) Å] and Ba-Cu_{MS} [4.790(10) Å] distances we can approximately determine Cu-O(2) distances near La and Ba atoms to be $\approx$2.414(20) Å and 2.250(16) Å, respectively (Fig. 8). An appropriate weighted average of these local configurations results in a Cu-O(2) distance of 2.404(18) Å in very good agreement with the 2.408(11) Å obtained in the Cu K-edge analysis [at $x=0.125$ the relative weights of having only La atoms at both ends ($\pm\hat{c}$) of Cu-O(2) bonds is $(1-x/2)^2=0.879$; one La and one Ba is $2(1-x/2)(x/2)=0.117$; only Ba atoms is $(x/2)^2=3.91\times10^{-3}$]. A similar weighted aver-

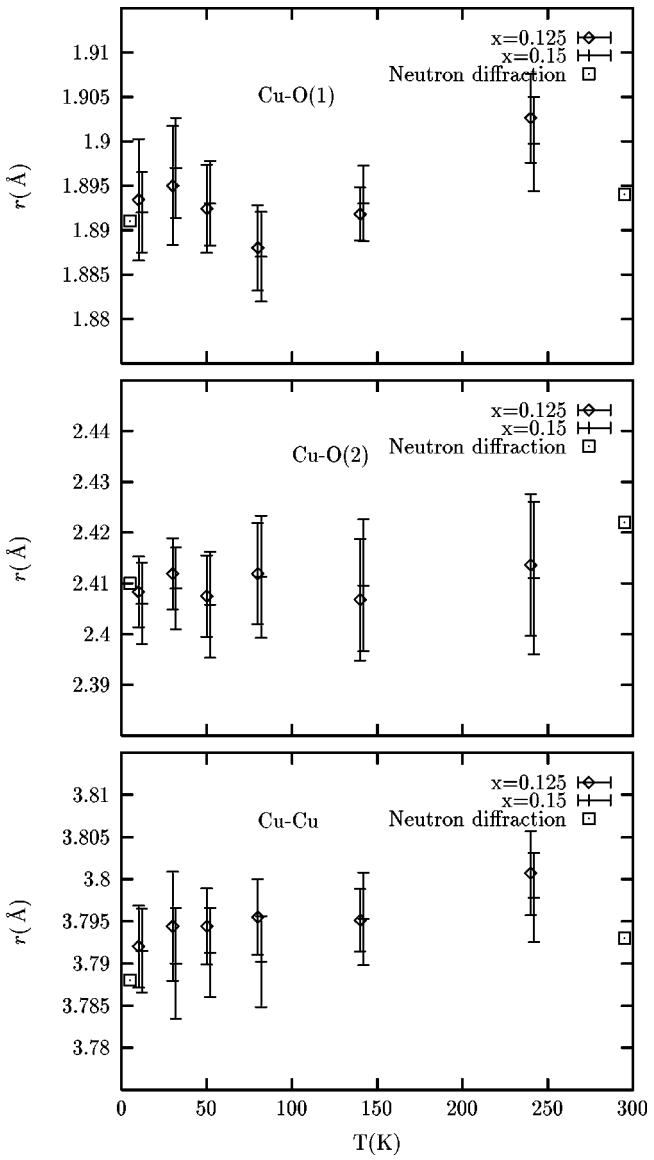

FIG. 17. Selected interatomic distances as obtained from Cu *K*-edge XAFS analysis. Correspondent neutron-diffraction values ($x=0.15$) (Ref. 33) at $T=10$ K (shown at 5 K for clarity) and 295 K also shown. Results for $x=0.15$ are displaced by 2 K for clarity.

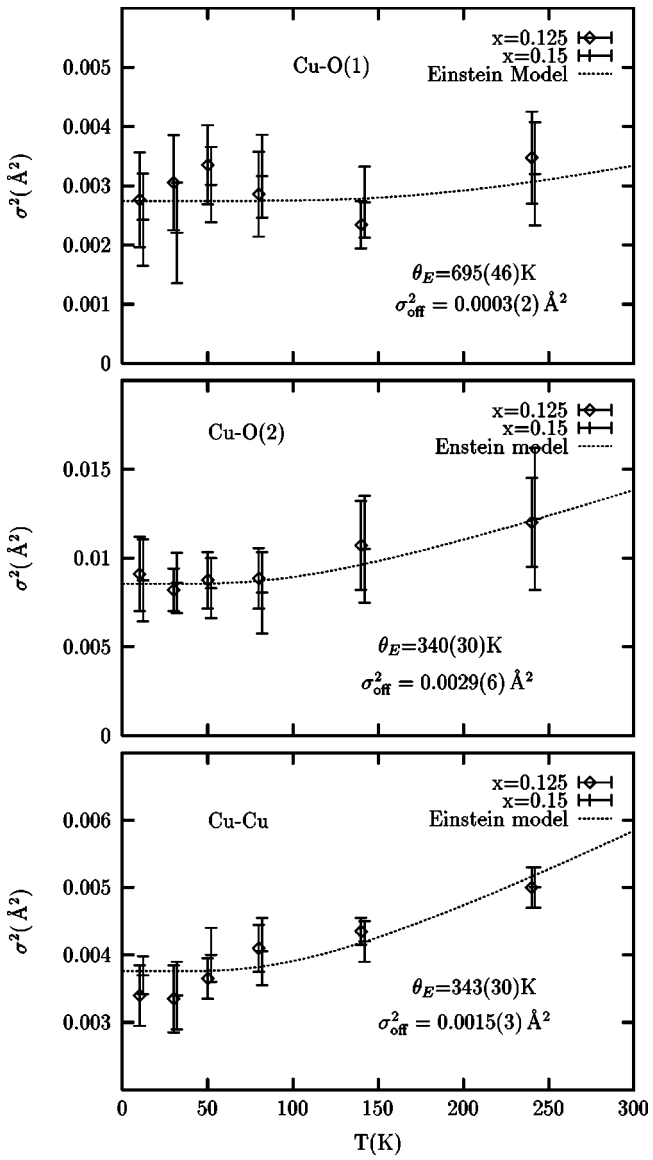

FIG. 18. σ^2 values for selected interatomic distances together with their fits to Einstein models using $x=0.125$ data. Static disorder $\sigma^2_{\rm off}$ needed to well fit the data also included. Results for $x=0.15$ are displaced by 2 K for clarity. An $S_0^2=0.91(6)$ value was obtained in the simultaneous refinements of both orientations.

age can be done to estimate the *static* MSD in bond length introduced by the different O(2) local configurations yielding $\sigma^2_{\rm off}=1.5\times10^{-3}$ Å^2. As pointed out in Sec. III D 1, Cu atoms neighboring Ba are locally displaced away from the dopants by ≈0.05 Å. Assuming these displacements are mostly along the $\hat{c}$ axis they would expand/contract (equally) Cu-O(2) distances about their average value since Ba substitution is random. This introduces additional static disorder of $\approx1.25\times10^{-3}$ Å^2 at $x=0.125$. Since the Cu and O(2) displacements are uncorrelated, the expected static disorder in Cu-O(2) distance is a $\sigma^2_{\rm off}\approx(1.5+1.25)\times10^{-3}$ Å$^2\approx2.75\times10^{-3}$ Å^2, in agreement with the result in Fig. 18.

The good fit of the MSD in Cu-O(1) bonds to an Einstein model with a small static offset contribution (Fig. 18) is consistent with our conjecture in Sec. III D 1 that the O(1,1′) and Cu local displacements nearby Ba dopants result in increased local buckling of the CuO_2 planes without significant changes in Cu-O(1,1′) bond lengths (estimated at $\lesssim0.005$ Å). On the other hand the $\sigma^2_{\rm off}$ obtained for the planar Cu-$Cu_{\rm MS}$ distance (Fig. 18) and for the Cu-$La_{\rm MS}$ distance along $\hat{c}$ (not shown) are too large to be accounted for by the Ba distortions. This static disorder reflects the unaccounted disorder in the buckling angle configuration of MS paths at nearly the same distances, as explained below.

2. Cu-O(2)-(La/Ba) and Cu-O(1,1′)-Cu three body correlations

To determine the extent of buckling angle fluctuations we followed the procedure described in Sec. III B 2. Since each of the MS signals of interest contributes in only one orientation direction we refined the structural parameters of Cu-O(2)-La/Ba and Cu-O(1,1′)-Cu MS paths, including buckling angle fluctuations, by fitting each orientation direction separately in the regions of *r*-space where these MS paths contribute significantly ($r=3.7-5$ Å and $r=3-4$ Å for

TABLE VIII. Einstein temperatures, θ_E; static disorder $\sigma^2_{\rm off}$, and goodness-of-fit parameters obtained for Cu-Cu_{MS} and Cu-La/Ba_{MS} paths for different modelings of local buckling angles. Fit results correspond to $x=0.125$ sample; results for $x=0.15$ are same within reported uncertainties. The total number of independent points in the data at six different temperatures is taken as six times the information content of each temperature data set.

Cu-O(1)-Cu					
Model	$\theta_E(K)$	$\sigma^2_{\rm off}$(Å ^{2})	N_I	N_P	χ^2_ν
$\alpha=5.9°$	357(35)	0.0018(3)	42	8	45.5
$\alpha=\alpha(T)$	296(14)	0.0002(7)	42	13	32.1
Cu-O(2)-La					
Model	$\theta_E(K)$	$\sigma^2_{\rm off}$(Å ^{2})	N_I	N_P	χ^2_ν
$\beta=6.9°$	158(16)	0.0030(06)	55	8	33.9
$\beta=\beta(T)$	174(24)	-0.0004(16)	55	13	23.58

$\hat{\epsilon}[\|,\perp]\hat{c}$, respectively). Structural parameters of all other paths were set to their values determined in the constrained fits of both orientations.

In contrast with the situation encountered at the La and Ba *K*-edges, additional nearly collinear MS paths contribute to the XAFS signal at about the same distance. These MS paths, however, involve at least two backscattering events compared to just one in Cu-O(2)-La/Ba and Cu-O(1,1′)-Cu MS paths. Although the contributions from Cu-O(2)-La/Ba and Cu-O(1,1′)-Cu SS, DS, and TS paths dominate the signal, as verified by our FEFF6 calculations,[47] all MS contributions were included in the fits. Distances and σ^2 for the additional, smaller, MS paths were related to those of SS paths without the need for additional structural parameters.[61] The important point to emphasize is that the SS and MS paths of interest dominate the signal and their structural parameters are not affected by the contributions of any other paths.

Data at T=10, 30, 50, 80, 140, 240 K were refined together by constraining the temperature dependence of σ^2 to follow an Einstein model but allowing for static disorder, $\sigma^2_{\rm off}$, as in Eq. (4). As before, a single σ^2 is refined for SS, DS, and TS paths at nearly the same distance. Effective scattering *amplitudes* are parametrized in terms of buckling angles while effective scattering *phases* are set to the values corresponding to the buckling angles of the average structure, $\langle\alpha\rangle=5.9°$, $\langle\beta\rangle=6.9°$ for Cu-O(1)-Cu and Cu-O(2)-La/Ba, respectively (Fig. 8). For the range of buckling angles considered here constraining the effective scattering phases introduces systematic errors in distance determination of $\lesssim 0.005$ Å but does not affect the measurement of buckling angles, as directly verified in our fits. MS half-path lengths are parametrized in terms of buckling angles and the SS half-path lengths, both of which are varied in the fits in addition to σ^2.

Table VIII compares fit results obtained by either constraining the local buckling angles to their average structure values or by allowing them to fluctuate. Similar to our findings in Sec. III B 2, while the former model results in too large $\sigma^2_{\rm off}$ values, their smaller values in the latter model are within our expectations based on the size of Ba induced distortions. In addition, fit improvements by varying the buckling angle are statistically significant as the ratio of χ^2_ν values obtained in both models is $\approx(1+2\sqrt{2/\nu})$ (2 standard deviations apart, Sec. III A), the fit with the lower χ^2_ν being better. Fit results in the region of *r*-space including the Cu-O(1)-Cu signal are shown for both models in Fig. 19. Our best fits give $\langle\alpha^2\rangle^{1/2}=13.1\pm2°$ and $\langle\beta^2\rangle^{1/2}=14.3\pm1.5°$ at $T=10$ K for Cu-O(1)-Cu and Cu-O(2)-La/Ba, respectively. The variations in these values with temperature or between $x=0.125,0.15$ samples are small and within the reported uncertainties.

Lack of significant temperature dependence in the buckling angle configuration of Cu-O(1,1′)-Cu has also been reported in the Cu *K*-edge XAFS study of unoriented powder of $La_{1.83}Ba_{0.17}CuO_4$ by Di Cicco and Sperandini.[62] This behavior is expected from the order-disorder nature of the temperature-induced phase transitions (Sec. III C).

Our fits indicate that essentially all of the static disorder in the three-body configurations can be accounted for by buckling angle fluctuations. However, one expects smaller contributions from other sources, e.g., disorder in SS and MS path

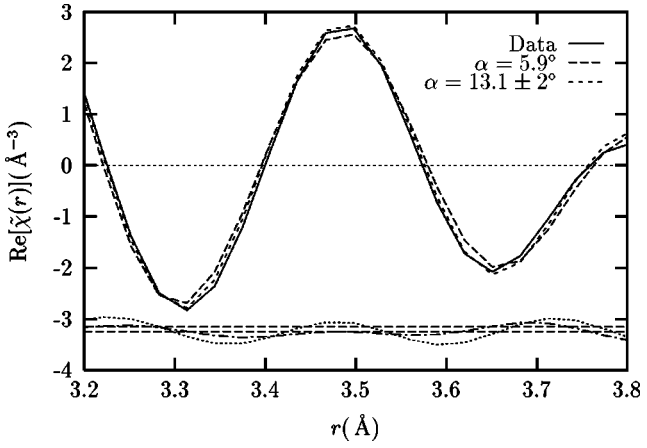

FIG. 19. Real part of the complex $\tilde{\chi}(r)$ for Cu *K*-edge, $\hat{a}$ polarization. The region of *r*-space including Cu-O(1)-Cu MS contributions is shown for fitting models with and without local buckling fluctuations. The MS signal peaks at ≈3.5 Å (instead of ≈3.78 Å) due to phase-shift effects in the p.e. final state; $\delta(k)$ in Eq. (1). Difference spectra also shown together with the level of *random* noise in the data (horizontal lines), taken as the rms of $\tilde{\chi}(r)$ in the range 15–25 Å where the XAFS signal is negligible.

lengths due to Ba distortions, but our data in Table VIII shows that their magnitude is hidden in the uncertainties of σ^2_{off}.

The slightly higher Einstein temperature of $\theta_E = 174(24)$ K obtained for Cu-La/Ba$_{\text{MS}}$ paths [zero-point motion of $\sigma^2_{\text{z.p.}} = 0.0030(5)$ Å^2] compared to the $\theta_E = 158(23)$ K of La-Cu$_{\text{MS}}$ paths from the La *K*-edge [$\sigma^2_{\text{z.p.}} = 0.0038(10)$ Å^2] is expected since Cu-Ba$_{\text{MS}}$ distances [$\theta_E = 204(10)$ K], which have less thermal disorder than the Cu-La$_{\text{MS}}$ ones, contribute to the Cu-La/Ba$_{\text{MS}}$ signal but not to the La-Cu$_{\text{MS}}$ one. Based on the La *K*-edge result that the local tilt angle, averaged over all majority atoms, agrees with its average structure value we obtain rms fluctuations in local buckling angles, $\langle \delta\alpha^2 \rangle^{1/2} = \langle (\alpha - \langle \alpha \rangle)^2 \rangle^{1/2}$ of $\langle \delta\alpha^2 \rangle^{1/2} = 2.0(3)\langle \alpha \rangle$ and $\langle \delta\beta^2 \rangle^{1/2} = 1.8(2)\langle \beta \rangle$ for Cu-O(1)-Cu and Cu-O(2)-La/Ba, respectively. The disorder in buckling angle of Cu-O(2)-La/Ba is consistent with that found for La-O(2)-Cu MS paths from La *K*-edge XAFS although smaller due to the contribution of the less statically disordered Cu-O(2)-Ba configuration to the former.

Since Cu-O(1)-Cu and Cu-O(2)-La/Ba signals contribute in different orientations, information about *correlations* between fluctuations about $\hat{a}\hat{a}$-plane and $\hat{c}$-axis (i.e., rigidity of CuO_6 octahedra tilt fluctuations) cannot be obtained from our measurements.

We note that in the modeling of Cu-O(1)-Cu correlations we assumed that O(1′) atoms remain in the CuO_2 planes as dictated by the average structure; i.e., that the Cu-O(1′)-Cu configuration is perfectly collinear. Ba-induced distortions, however, affect both O(1, 1′) atoms. In particular O(1′) atoms nearby Ba are displaced out of the CuO_2 planes (Sec. III D 1). Our fitting result therefore overestimates the disorder in buckling angle of Cu-O(1)-Cu configuration since it compensates for unaccounted disorder in Cu-O(1′)-Cu MS paths. A better estimate can be obtained by allowing buckling disorder in both Cu-O(1)-Cu and Cu-O(1′)-Cu MS paths. Since we cannot distinguish between these paths, we can only obtain an averaged disorder in CuO_2 planar buckling angle. By doing so we obtain a fit of the same quality as before ($\chi^2_\nu = 32.5$; we cannot distinguish between the two models) but now $\langle \alpha^2 \rangle^{1/2}_{\text{plane}} = 8.7 \pm 2°$ resulting in rms buckling angle fluctuations of CuO_2 planes of $\langle \delta\alpha^2 \rangle^{1/2}_{\text{plane}} = 1.4(3)\langle \alpha \rangle$.

Evidence for large disorder in the buckling angle of CuO_2 planes is also found in Ref. 62, where a *mean* buckling angle of $\approx 12°$, with rms deviation of about 2°, is reported. As noted by the authors, this large *mean* angle is in disagreement with the results of crystallography[13,14] [mean buckling angle of CuO_2 planes $\approx (5.9°/2) \approx 3°$]. Since the (nearly) forward scattering amplitude at the O(1,1′) sites is only sensitive to $\langle \alpha^2 \rangle_{\text{plane}}$, the XAFS measurement at the Cu site alone cannot distinguish between a large mean buckling angle or large random fluctuations in its value (Sec. III B 2). The results of Ref. 62 yield $\langle \alpha^2 \rangle^{1/2}_{\text{plane}} \approx 12 \pm 2°$, in quite good agreement with our value of $\langle \alpha^2 \rangle^{1/2}_{\text{plane}} = 8.7 \pm 2°$.

IV. DISCUSSION

A. On the plausibility of a density of states effect as the basis of T_c suppression at $x = 0.125$

The first moment of the *local* LTT tilt angle of CuO_6 octahedra, as determined from La XAFS, is $\langle \theta \rangle = 3.3(4)°$ in good agreement with the results of diffraction techniques.[13,14,63] As band-structure calculations by Norman *et al.* clearly showed,[12] this tilt angle is not large enough to cause a significant effect on the density of states (DOS) at the Fermi energy (E_F) when going from the LTO to the LTT phase. The minor effect that the appearance of the LTT phase has on the DOS(E_F) for such magnitude of tilts is confirmed by photoemission studies on single crystals of $La_{1.875}Ba_{0.125}CuO_4$ showing no significant change in the DOS(E_F) when cooling through the LTO to LTT transition.[64]

The splitting of the van Hove peak resulting in a decrease of the DOS(E_F) (for $x = 0.125$) by about a factor of 2 initially suggested by Pickett, Cohen, and Krakauer (PCK) (Ref. 10) as the cause of T_c suppression appears at much larger tilt angles (≈ 2 times larger).[15] For such larger angles, a gap appears precisely at E_F for $x = 0.125$ all along a Brillouin zone (BZ) edge (the *M*-*A* edge). The band splitting, which originates in the inequivalent O(1,1′) atoms in the LTT phase (those moving out of the CuO_2 planes compared to those staying in the plane), reflects a strong hole-lattice interaction for these Fermi surface states, which increases quadratically with tilt angle[11] (and thus with buckling angle α). Because of this hole-lattice interaction, the large disorder in tilt angles causes a strong scattering of the Fermi surface states along the *M*-*A* edge of the BZ and not a gap, which requires a periodic distortion. It is possible that these states could become localized by the random disorder, producing a *mobility* gap along the *M*-*A* edge (other states at E_F are not affected). The calculations of PCK suggest that as much as half of the states at the Fermi energy could be in this mobility gap. Such states would not contribute to superconductivity, leading to T_c suppression. Despite both the local (this work) and average (Ref. 52) structures of $x = 0.125$,0.15 samples being very similar (and therefore so are their rigid band electronic structures), doping from $x = 0.125$ to $x = 0.15$ moves the chemical potential (in a rigid band picture) from the localized states in the mobility gap to the mobile states outside.

In this scenario the DOS(E_F) would not decrease at the LTO to LTT transition (consistent with experiment) but rather the density of *mobile* states at E_F (for $x = 0.125$) will be reduced when the long-range LTT order appears. This conjecture seems to be supported by the increase in electrical resistivity when cooling into the LTT phase[2,3] indicative of enhanced scattering and possible localization of carriers, although details on what type of activation process rules the conductivity are masked by the appearance of superconductivity at low temperatures. That bulk superconductivity is observed at $x = 0.125$, although with reduced T_c and superconducting volume fraction, is consistent with only a fraction of the Fermi surface states becoming immobilized by disorder. Since DOS features (including a mobility gap) will be broadened by disorder and by electron-phonon and electron-electron interactions, one would expect a broadened regime of x values around $x = 0.125$ showing suppressed superconductivity, in agreement with experiment.[2] This model gives an explanation of why T_c suppression occurs only near $x = 0.125$ and for the LTT phase.

The question remains whether such a mechanism could explain the T_c suppression observed in other cuprates at x

$\sim$1/8 including $La_{1.48}Nd_{0.4}Sr_{0.12}CuO_4$, which exhibits charge and spin stripe ordering[4] and no bulk superconductivity,[37] and $La_{1.88}Sr_{0.12}CuO_4$ for which a small ($\approx$10%) LTT fractional volume is observed to accompany a small T_c suppression.[65–67] Whereas it seems unlikely that these systems will all exhibit similarly large disorder [the mismatch of ionic radii of Nd^{+3} (1.16 Å) and Sr^{+2} (1.31 Å) with La^{+3} (1.22 Å) is smaller than for Ba^{+2} (1.47 Å), Ref. 60], the similarly large thermal ellipsoids obtained for O(2) atoms in the neutron-diffraction refinements[68] of $La_{1.48}Nd_{0.4}Sr_{0.12}CuO_4$ and $La_{1.88}Ba_{0.12}CuO_4$ could indicate the presence of large intrinsic disorder also in the Nd-doped sample. The disorder observed in the stripe spacing of this material[18] would be consistent with the presence of structural disorder, although the local, random, potential variations introduced by a charged Sr^{+2} dopant could also explain the disorder in the charge stripe spacing[18]. While the extent of structural disorder induced by Sr substitution is, although significant, much smaller than that induced by Ba (this work and Refs. 53 and 58), a quantitative measure of the local disorder induced by Nd in $La_{1.48}Nd_{0.4}Sr_{0.12}CuO_4$ is currently lacking to fully address this point.

We note that the Anderson critical value[69,70] of the strength of the random component of the scattering potential, V_0, needed for localization, $(V_0/B)_{\rm crit}$, where B is the bandwidth, would be reduced in the highly anisotropic cuprates due to their smaller overlap energy integrals and narrow bandwidths.[70]

B. On the effect of disorder on charge and spin ordering

Our findings indicate that the nature of disorder introduced with Ba substitution goes well beyond the random variation in local potential due to the different charge states of Ba^{+2} and La^{+3} ions. Ba doping introduces local structural distortions, which severely change the corrugation pattern of CuO_2 planes and of octahedral tilts near a Ba dopant. Since both charge and spin degrees of freedom couple to octahedral tilts (the latter via spin-orbit interaction and superexchange dependence on the buckling angle α)[17,71] it is expected that this intrinsic, random, disorder will frustrate long-range ordering of charge and spins.[21,72] Short-range charge and spin ordering, however, if energetically favorable, will persist even in the presence of disorder, although correlation lengths will be largely determined by the nature of this disorder. It is not surprising, therefore, that strong evidence for spin and charge stripe ordering in $La_{1.875}Ba_{0.125}CuO_4$ has so far only been found by techniques that probe local ordering, such as μSR (Refs. 22 and 23) and NQR.[25] It should be mentioned that the search for such ordering by neutron-scattering measurements has been limited by the lack of large single crystalline samples. The magnitude of the ordered Cu moment observed by μSR below about 30 K in $La_{1.875}Ba_{0.125}CuO_4$ and $La_{1.48}Nd_{0.4}Sr_{0.12}CuO_4$, $\approx 0.34\mu_B$, is about three times larger than the value obtained from neutron scattering measurements, consistent with the presence of disorder in the spin modulation.[23,24] Tranquada *et al.*[18] estimated the correlation length of such spin ordering in $La_{1.48}Nd_{0.4}Sr_{0.12}CuO_4$ to be $\approx$200 Å (below 30 K). The large structural disorder introduced with Ba doping could result in even shorter correlation lengths in $La_{1.875}Ba_{0.125}CuO_4$. For example, the average distance between randomly located Ba dopants in a La_2O_2 plane, which determines the distance between severely distorted regions of CuO_2 planes, is $\approx$15 Å. A theoretical discussion on the effect of disorder on striped phases can be found in Refs. 21 and 73.

A study of the magnetic dynamics in La_2CuO_4 and $La_{1.95}Ba_{0.05}CuO_4$ samples by inelastic neutron scattering[74] revealed, in addition to the presence of antiferromagnetic (AFM) spin wave softening due to hole doping of the CuO_2 planes (decrease in spin wave velocity) the presence of substantial AFM spin wave *damping* in the Ba-doped sample. The large local fluctuations in buckling angle of CuO_2 planes introduced with Ba doping will effectively scatter these spin waves and could be responsible for their measured decay rate.[74]

Evidence for local charge ordering in $La_{1.875}Ba_{0.125}CuO_4$, with a local charge distribution similar to that observed in $La_{1.48}Nd_{0.4}Sr_{0.12}CuO_4$, comes from recent ^{63}Cu nuclear quadrupole resonance (NQR) measurements.[25] Based on the estimates from neutron-scattering measurements[24] for the amplitude of local atomic displacements commensurate with such charge ordering, we concluded in Sec. I that the XAFS signal will be almost unaffected by such ordering. Figures 17 and 18 support this conclusion as no significant anomaly is detected, within uncertainties, in the temperature dependencies of the Cu-O(1,1′) distances and their mean-squared displacements, σ^2, below the appearance of the LTT phase ($\approx$60 K). Although the data could be consistent with some anomalous behavior, e.g., a slight expansion by $\lesssim$0.01 Å of the Cu-O(1,1′) distance below $\approx$80 K and/or a slight broadening in the Cu-O(1,1′) distribution by $\lesssim$0.001 Å^2 at about the same temperature, these deviations are not significant compared to the XAFS error and any such conclusion is highly speculative. The systematic increase, of about 0.0018 Å^2, in σ^2 of Cu-O(1,1′) distances below about 80 K reported in the *unoriented* powder XAFS study of Ref. 75, is inconsistent with our data. Although the reason for this discrepancy is unclear at present, possible origins include the underestimation of uncertainties in structural parameters and/or the neglect of the Cu-O(2) apical signal in the analysis of Cu-O (planar) correlations in Ref. 75. Our data on *oriented* powder alleviates these shortcomings for the reasons detailed in Sec. III E 1.

Although our XAFS measurements cannot detect and, thus, address the existence of charge stripe ordering in $La_{2-x}Ba_xCuO_4$, an upper limit on the extent of local atomic displacements commensurate with charge ordering can be given from the size of the residual $\sigma^2_{\rm off}=3(2)\times10^{-4}$ Å^2 in the disorder of the Cu-O (planar) distance after an Einstein model fit to its temperature dependence resulting in an rms disorder, averaged over all Cu atoms, of $\lesssim$0.017 Å. This estimate holds whether the displacements are pinned by the lattice at $x=0.125$ or dynamic at $x=0.15$, as the fast XAFS technique (characteristic time scale $\approx10^{-15}$ sec.) cannot distinguish between static and dynamic atomic displacements.

V. SUMMARY AND CONCLUSIONS

Angular dependent XAFS measurements on *oriented* powder of $La_{2-x}Ba_xCuO_4$ with $x=0.125,0.15$ at $T=10$ K

show that local tilts of CuO_6 octahedra are predominantly LTT-like, with an upper limit for the fraction of LTO local tilts within the LTT ground state of $\lesssim 10\%$. While the local symmetry at $T=10$ K is the same as that of the long-range averaged structure, a large amount of intrinsic disorder is present in the LTT ground state. This disorder originates in ≈ 5 Å distorted regions around Ba dopant sites, which include large local changes in the corrugation pattern of CuO_2 planes. Despite the low Ba content, a significant fraction of the lattice is affected by the large local distortions. The intrinsic disorder manifests a random local fluctuation of the LTT tilt angle of CuO_6 octahedra with an rms, averaged over all La and Cu majority atoms, of $\langle(\theta-\langle\theta\rangle)^2\rangle^{1/2}\approx 2\langle\theta\rangle$, $\langle\theta\rangle$ being the tilt angle determined by diffraction studies.

While indications of structural disorder in the LTT phase of $La_{2-x}Ba_xCuO_4$ have been previously reported, e.g., convergent beam electron diffraction studies[76] at $T=15$ K showed lattice parameter variations on a $\approx 100-300$ Å scale, our measurements provide detailed information on the nature of intrinsic disorder at length scales comparable to the superconducting coherence length, $\zeta_{SC}\approx 10$ Å. This information should provide a more quantitative base for a better assessment of the role played by disorder in determining normal and superconducting properties of $La_{2-x}Ba_xCuO_4$.

La *K*-edge measurements show that the local tilts do not change their orientation during the LTT $\rightarrow$ LTO transition, but remain tilted as in the LTT configuration even at the higher temperatures of the HTT phase. Temperature, therefore, introduces extra disorder with the long-range LTO and HTT structures resulting from local LTT regions of intermediate size becoming uncorrelated in their tilts. This is in agreement with previous findings by PDF analysis of neutron-scattering data.[51] The order-disorder nature of the LTT $\rightarrow$ LTO $\rightarrow$ HTT phase transitions that follows from these results is in agreement with the LDA energy surfaces obtained for $La_{2-x}Ba_xCuO_4$ in Ref. 10.

A direct comparison of $x=(0.125,0.15)$ samples at $T=10$ K indicates no significant differences between their local structures (≈ 5 Å scale) beyond that expected from the small changes in lattice parameters. Our measurements at the Cu *K*-edge put an upper limit of $\Delta r\lesssim 0.005$ Å for the difference in interatomic distances in the two samples, up to the fifth shell of atoms. Since their average structures are also nearly the same,[52,51] changes in structural properties are not sufficient to explain T_c suppression at $x=0.125$ and a significant change in electronic structure with doping is required. We discussed our results in the context of two possible such mechanisms, which may be related: (a) disorder induced localization of a large fraction of Fermi surface states that occurs only when the Fermi surface coincides with the *M*-*A* zone edge of the BZ at $x=0.125$ in the LTT phase and (b) static stripe formation. It is reasonable to assume that a common mechanism for T_c suppression at $x\sim 1/8$ can be found for all such suppressed superconducting cuprates. In this respect it is desirable to obtain information on the extent of local structural disorder introduced with Nd in $La_{1.48}Nd_{0.4}Sr_{0.12}CuO_4$ to assess the validity of (a). The mobility gap scenario, which results from combining the large local disorder found by XAFS with knowledge from the LDA band-structure calculations[10] provides a natural explanation for why T_c suppression occurs at $x=1/8$ *and* only in the LTT phase of cuprates with an attendant increase in carrier-lattice scattering.

The large disorder of $La_{2-x}Ba_xCuO_4$ will frustrate charge and spin stripe ordering over long range, although recent experimental evidence from local probes indicate that such ordering exists locally. Our XAFS results are not inconsistent with such ordering and put an upper limit of $\lesssim 0.017$ Å, averaged over all Cu atoms, on the rms displacements of Cu-O(planar) distances commensurate with such spin and charge ordering, whether static at $x=0.125$ or dynamic at $x=0.15$. We notice that (a) and (b) are not exclusive mechanisms so that disorder could, in principle, contribute to the pinning of static stripes at $x=0.125$.

ACKNOWLEDGMENTS

We acknowledge helpful discussions with J. Tranquada, V. Emery, S. Billinge, T. Egami, S. Heald, and N. Sicron. The valuable help of F. Perez and M. Suenaga in orienting the samples is greatly appreciated. Work at the University of Washington (D.H. and E.A.S.) was done under auspices of DOE Grant No. DE-FG03-98ER45681 while work at BNL was supported by DOE Grant No. DE-AC02-98CH10886.

*Present address: Advanced Photon Source, Bldg. 401, Argonne National Laboratory, Argonne, IL 60439.

[1] J. D. Axe, A. H. Moudden, D. Hohlwein, D. E. Cox, K. M. Mohanty, A. R. Moodenbaugh, and Youwen Xu, Phys. Rev. Lett. **62**, 2751 (1989).

[2] A. R. Moodenbaugh, Youwen Xu, M. Suenaga, T. J. Folkerts, and R. N. Shelton, Phys. Rev. B **38**, 4596 (1988).

[3] M. Sera, Y. Ando, S. Kondoh, K. Fukuda, M. Sato, I. Watanabe, S. Nakashima, and K. Kumagi, Solid State Commun. **69**, 851 (1989).

[4] J. M. Tranquada, B. J. Sternlieb, J. D. Axe, Y. Nakamura, and S. Uchida, Nature (London) **375**, 561 (1995); J. M. Tranquada, D. J. Buttrey, V. Sachan, and J. E. Lorenzo, Phys. Rev. Lett. **73**, 1003 (1994).

[5] Y. Nakamura and S. Uchida, Phys. Rev. B **46**, 5841 (1992).

[6] S. Katano, S. Funahashi, N. Môri, Y. Ueda, and J. A. Fernandez-Baca, Phys. Rev. B **48**, 6569 (1993).

[7] S. Katano, Y. Ueda, A. Hayashi, and N. Môri, Physica B **213&214**, 81 (1995).

[8] Y. Maeno, N. Kakehi, M. Kato, and T. Fujita, Phys. Rev. B **44**, 7753 (1991).

[9] A. R. Moodenbaugh, U. Wildgruber, Y. L. Wang, and Youwen Xu, Physica C **245**, 347 (1995).

[10] W. E. Pickett, R. E. Cohen, and H. Krakauer, Phys. Rev. Lett. **67**, 228 (1991).

[11] S. Barisic and J. Zelenko, Solid State Commun. **74**, 367 (1990); **74**, 228 (1991).

[12] M. R. Norman, G. J. McMullan, D. L. Novikov, and A. J. Freeman, Phys. Rev. B **48**, 9935 (1993).

[13] S. Katano, J. A. Fernandez-Baca, S. Funahashi, N. Môri, Y. Ueda, and K. Koga, Physica C **214**, 64 (1993).

[14] E. Takayama-Muromachi, F. Izumi, and T. Kamiyama, Physica C **215**, 329 (1993).

[15] W. E. Pickett, R. E. Cohen, and H. Krakauer, Physica B **169**, 45 (1991).
[16] R. E. Cohen, W. E. Pickett, D. Papaconstantopoulos, and H. Krakauer, in *Lattice Effects in High T_c Superconductors*, edited by Y. Bar Yam, T. Egami, J. Mustre de Leon, and A. R. Bishop (World Scientific, Singapore, 1992).
[17] N. E. Bonesteel, T. M. Rice, and F. C. Zhang, Phys. Rev. Lett. **68**, 2684 (1992).
[18] J. M. Tranquada, N. Ichikawa, and S. Uchida, Phys. Rev. B **59**, 14 712 (1999).
[19] V. J. Emery, S. A. Kivelson, and O. Zachar, Phys. Rev. B **56**, 6120 (1997).
[20] V. J. Emery, Physica B **169**, 17 (1991).
[21] S. A. Kivelson, E. Fradkin, and V. J. Emery, Nature (London) **393**, 550 (1998).
[22] G. M. Luke, L. P. Le, B. J. Sternlieb, W. D. Wu, Y. J. Uemura, J. H. Brewer, T. M. Riseman, S. Ishibashi, and S. Uchida, Physica C **185-189**, 1175 (1991); K. Kumagai, I. Watanabe, K. Kawano, H. Matoba, K. Nishiyama, K. Nagamine, N. Wada, M. Okaji, and K. Nara, *ibid.* **185-189**, 913 (1991).
[23] B. Nachumi, Y. Fudamoto, A. Keren, K. M. Kojima, M. Larkin, G. M. Luke, J. Merrin, O. Tchernyshyov, Y. J. Uemura, N. Ichikawa, G. Goto, H. Takagi, S. Uchida, M. K. Crawford, E. M. McCarron, D. E. MacLaughlin, and R. H. Heffner, Phys. Rev. B **58**, 8760 (1998).
[24] J. M. Tranquada, J. D. Axe, N. Ichikawa, Y. Nakamura, S. Uchida, and B. Nachumi, Phys. Rev. B **54**, 7489 (1996).
[25] A. W. Hunt, P. M. Singer, K. R. Thurber, and T. Imai, Phys. Rev. Lett. **82**, 4300 (1999).
[26] The XAFS MSD can be written as $\sigma_{ij}^2=\langle(\vec{r}_j'-\vec{r}_j)^2\rangle_{j'}+\langle(\vec{r}_i'-\vec{r}_i)^2\rangle_{i'}-2\langle(\vec{r}_j'-\vec{r}_j)\cdot(\vec{r}_i'-\vec{r}_i)\rangle_{j',i'}$, where $\vec{r}_i'$, $\vec{r}_i$ are the instantaneous and lattice positions for atom i and $\langle\ \rangle$ are configurational averages over the distribution of instantaneous positions. For equal and anticorrelated motions of i,j, $\sigma_{ij}^2=4u_i^2$, with u_i^2 the mean squared disorder of each atom in the pair relative to its lattice site.
[27] John Rehr (private communication).
[28] J. M. Tranquada, J. E. Lorenzo, D. J. Buttrey, and V. Sachan, Phys. Rev. B **52**, 3581 (1995).
[29] T. Niemöller, B. Büchner, M. Cramm, C. Huhnt, L. Tröger, and M. Tischer, Physica C **299**, 191 (1998).
[30] D. Haskel, E. A. Stern, and H. Shechter, Phys. Rev. B **57**, 8034 (1998).
[31] K. Fukuda, S. Shamoto, M. Sato, and K. Oka, Solid State Commun. **65**, 1323 (1988).
[32] O. B. Hyun, S. C. Sanders, and D. K. Finnemore, J. Supercond. **2**, 529 (1989).
[33] J. D. Jorgensen, H.-B. Schüttler, D. G. Hinks, D. W. Capone II, K. Zhang, M. B. Brodsky, and D. J. Scalapino, Phys. Rev. Lett. **58**, 1024 (1987).
[34] C. Rial, E. Moran, M. A. Alario-Franco, U. Amador, and N. H. Andersen, Physica C **270**, 51 (1996).
[35] T. Nagano, Y. Tomioka, Y. Nakayama, K. Kishio, and K. Kitazawa, Phys. Rev. B **48**, 9689 (1993).
[36] Q. Li, M. Suenaga, T. Kimura, and K. Kishio, Phys. Rev. B **47**, 2854 (1993).
[37] A. R. Moodenbaugh, L. H. Lewis, and S. Soman, Physica C **290**, 98 (1997).
[38] J. R. Clem, Physica C **153-155**, 50 (1988).
[39] Y. Zhu, A. R. Moodenbaugh, Z. X. Cai, J. Tafto, M. Suenaga, and D. O. Welch, Phys. Rev. Lett. **73**, 3026 (1987).
[40] O. Keski-Rahkonen and M. O. Krause, At. Data Nucl. Data Tables **14**, 139 (1974).
[41] A. Hofmann, SSRL Report No. ACD-NOTE 38, 1986 (unpublished).
[42] E. A. Stern and K. Kim, Phys. Rev. B **23**, 3781 (1981).
[43] E. A. Stern, Phys. Rev. B **10**, 3027 (1974).
[44] J. J. Rehr, R. C. Albers, C. R. Natoli, and E. A. Stern, Phys. Rev. B **34**, 4350 (1986); J. J. Rehr, E. A. Stern, R. L. Martin, and E. R. Davidson, *ibid.* **17**, 560 (1978).
[45] P. A. Lee and J. B. Pendry, Phys. Rev. B **11**, 2795 (1975).
[46] J. J. Rehr and R. C. Albers, Phys. Rev. B **41**, 8139 (1990); J. J. Rehr, R. C. Albers, and S. I. Zabinsky, Phys. Rev. Lett. **69**, 3397 (1992).
[47] S. Zabinsky, J. J. Rehr, A. Ankudinov, R. C. Albers, and M. J. Eller, Phys. Rev. B **52**, 2995 (1995).
[48] E. A. Stern, M. Newville, B. Ravel, Y. Yacoby, and D. Haskel, Physica B **208&209**, 117 (1995).
[49] E. A. Stern, Phys. Rev. B **48**, 9825 (1993).
[50] M. Newville, B. Ravel, D. Haskel, J. J. Rehr, E. A. Stern, and Y. Yacoby, Physica B **208&209**, 154 (1995).
[51] S. J. Billinge, G. H. Kwei, and H. Takagi, Phys. Rev. Lett. **72**, 2282 (1994).
[52] S. J. L. Billinge, G. H. Kwei, A. C. Lawson, J. D. Thompson, and H. Takagi, Phys. Rev. Lett. **71**, 1903 (1993).
[53] D. Haskel, E. A. Stern, D. G. Hinks, A. W. Mitchell, J. D. Jorgensen, and J. I. Budnick, Phys. Rev. Lett. **76**, 439 (1996).
[54] A. Frenkel, E. A. Stern, A. Voronel, M. Quian, and M. Newville, Phys. Rev. B **49**, 11 662 (1994); B. Rechav, Y. Yacoby, E. A. Stern, J. J. Rehr, and M. Newville, Phys. Rev. Lett. **72**, 1352 (1994).
[55] Configurations with different buckling angles are constructed by displacing the O(2) atoms *perpendicular* to the $\hat{c}$ axis by a vector $(x,x,0)$. The β^2 dependence in $F_k(\beta)=F_k(\langle\beta\rangle)(\gamma_k+\zeta_k\beta^2)$ is exact only if the three-atom configuration is unchanged under $(x,x,0)\rightarrow-(x,x,0)$. The planar off-center displacement of La atoms (≈ 0.04 Å from the $\hat{c}$ axis) breaks this symmetry and the actual dependence fits $\beta^{1.91}$ (with accordingly different γ_k,ζ_k coefficients). Similar arguments hold for the β dependence of half-path lengths. We used the exact parametrization for the half-path lengths and β^2 for the scattering amplitude's corrections. The difference in the amplitude correction due to the latter is about 5% and did not affect the fit results for β, within uncertainties. For the case where $\langle\beta\rangle=0$, $\gamma_k\equiv 1$.
[56] E. Sevillano, H. Meuth, and J. J. Rehr, Phys. Rev. B **20**, 4908 (1979).
[57] P. G. Radaelli, D. G. Hinks, A. W. Mitchell, B. A. Hunter, J. L. Wagner, B. Dabrowski, K. G. Vandervoort, H. K. Viswanathan, and J. D. Jorgensen, Phys. Rev. B **49**, 4163 (1994).
[58] D. Haskel, E. A. Stern, D. G. Hinks, A. W. Mitchell, and J. D. Jorgensen, Phys. Rev. B **56**, R521 (1997).
[59] T. Egami, W. Dmowski, J. D. Jorgensen, D. G. Hinks, D. W. Capone II, C. U. Segre, and K. Zhang, Rev. Solid State Sci. **1**, 247 (1987).
[60] R. D. Shannon, Acta Crystallogr., Sect. A: Cryst. Phys., Diffr., Theor. Gen. Crystallogr. **32**, 751 (1976).
[61] D. Haskel, Ph.D. thesis, University of Washington, 1998.
[62] A. Di Cicco and F. Sperandini, Physica C **258**, 349 (1996).
[63] D. E. Cox *et al.*, in *High Temperature Superconductors: Relationships Between Properties, Structure, and Solid-State Chemistry*, edited by J. R. Jorgensen *et al.*, MRS Symposia Proceed-

ings No. 156 (Materials Research Society, Pittsburgh, 1989), p. 141.
[64] T. Maruyama, Y. Aiura, Y. Nishihara, T. Ito, K. Oka, Y. Ohashi, Y. Haruyama, and H. Kato, Physica C **235-240**, 1049 (1994).
[65] A. R. Moodenbaugh, L. Wu, Y. Zhu, L. H. Lewis, and D. E. Cox, Phys. Rev. B **58**, 9549 (1998).
[66] Y. Horibe, Y. Inoue, and Y. Koyama, Physica C **282-287**, 1071 (1997).
[67] Y. Inoue, Y. Horibe, and Y. Koyama, J. Supercond. **10**, 361 (1997).
[68] J. D. Axe and M. K. Crawford, J. Low Temp. Phys. **95**, 271 (1994).
[69] P. W. Anderson, Phys. Rev. **109**, 1492 (1958).
[70] N. F. Mott, in *Metal-Insulator Transitions*, 2nd ed. (Taylor & Francis, London, 1990).
[71] T. Thio, T. R. Thurston, N. W. Preyer, P. J. Picone, M. A. Kastner, H. P. Jenssen, D. R. Gabbe, C. Y. Chen, R. J. Birgeneau, and A. Aharony, Phys. Rev. B **38**, 905 (1988).
[72] A. I. Larkin, Zh. Éksp. Teor. Fiz. **58**, 1466 (1970) [Sov. Phys. JETP **31**, 784 (1970)].
[73] N. Hasselmann, A. H. Castro Neto, C. Morais Smith, and Y. Dimashko, Phys. Rev. Lett. **82**, 2135 (1999).
[74] G. Aeppli, S. M. Hayden, H. A. Mook, Z. Fisk, S-W. Cheong, D. Rytz, J. P. Remeika, G. P. Espinosa, and A. S. Cooper, Phys. Rev. Lett. **62**, 2052 (1989).
[75] A. Lanzara, N. L. Saini, T. Rossetti, A. Bianconi, H. Oyanagi, H. Yamaguchi, and Y. Maeno, Solid State Commun. **97**, 93 (1996).
[76] C. H. Chen, S-W. Cheong, D. J. Werder, A. S. Cooper, and L. W. Rupp, Jr., Physica C **175**, 301 (1991).